atmosphere

MDPI

Article

Phosphate Buffer Solubility and Oxidative Potential of Single Metals or Multielement Particles of Welding Fumes

Manuella Ghanem [1,2], Esperanza Perdrix [2], Laurent Yves Alleman [2], Davy Rousset [1,*] and Patrice Coddeville [2]

[1] Department of Pollutant Metrology, Institut National de Recherche et de Sécurité (INRS), 54500 Vandœuvre-lès-Nancy, France; manuella.ghanem@inrs.fr
[2] Center for Energy and Environment, IMT Lille Douai, Institut Mines-Télécom, University of Lille, 59000 Lille, France; esperanza.perdrix@imt-lille-douai.fr (E.P.); laurent.alleman@imt-lille-douai.fr (L.Y.A.); patrice.coddeville@imt-lille-douai.fr (P.C.)
* Correspondence: davy.rousset@inrs.fr

Abstract: To evaluate the chemical behavior and the health impact of welding fumes (WF), a complex and heterogeneous mixture of particulate metal oxides, two certified reference materials (CRMs) were tested: mild steel WF (MSWF-1) and stainless steel WF (SSWF-1). We determined their total chemical composition, their solubility, and their oxidative potential in a phosphate buffer (PB) solution under physiological conditions (pH 7.4 and 37 °C). The oxidative potential (OP^{DTT}) of WF CRMs was evaluated using an acellular method by following the dithiothreitol (DTT) consumption rate (µmol DTT L^{-1} min^{-1}). Pure metal salts present in the PB soluble fraction of the WF CRMs were tested individually at equivalent molarity to estimate their specific contribution to the total OP^{DTT}. The metal composition of MSWF-1 consisted mainly of Fe, Zn, Mn, and Cu and the SSWF-1 composition consisted mainly of Fe, Mn, Cr, Ni, Cu, and Zn, in diminishing order. The metal PB solubility decreased from Cu (11%) to Fe (approximately 0.2%) for MSWF-1 and from Mn (9%) to Fe (<1%) for SSWF-1. The total OP^{DTT} of SSWF-1 is 2.2 times the OP^{DTT} of MSWF-1 due to the difference in oxidative capacity of soluble transition metals. Cu (II) and Mn (II) are the most sensitive towards DTT while Cr (VI), Fe (III), and Zn (II) are barely reactive, even at higher concentrations. The OP^{DTT} measured for both WF CRMs extracts compare well with simulated extracts containing the main metals at their respective PB-soluble concentrations. The most soluble transition metals in the simulated extract, Mn (II) and Cu (II), were the main contributors to OP^{DTT} in WF CRMs extracts. Mn (II), Cu (II), and Ni (II) might enhance the DTT oxidation by a redox catalytic reaction. However, summing the main individual soluble metal DTT response induces a large overestimation probably linked to modifications in the speciation of various metals when mixed. The complexation of metals with different ligands present in solution and the interaction between metals in the PB-soluble fraction are important phenomena that can influence OP^{DTT} depletion and therefore the potential health effect of inhaled WF.

Keywords: oxidative potential; DTT; phosphate buffer solubility; metal; welding fumes; particles

Citation: Ghanem, M.; Perdrix, E.; Alleman, L.Y.; Rousset, D.; Coddeville, P. Phosphate Buffer Solubility and Oxidative Potential of Single Metals or Multielement Particles of Welding Fumes. *Atmosphere* **2021**, *12*, 30. https://doi.org/10.3390/atmos12010030

Received: 18 November 2020
Accepted: 23 December 2020
Published: 28 December 2020

1. Introduction

Inhalation exposure to welding fumes can have a significant health impact on welders and nearby workers [1]. There are around 11 million welders worldwide, and around 110 million additional workers are likely to be exposed to welding fumes [2], either working in open and well-ventilated environments (e.g., outdoor construction sites) or in confined and poorly ventilated ones (e.g., ship hulls, crawl spaces of buildings, and pipelines) [3]. This activity is in constant growth, as stated by the Office of Labor Statistics of the United States in 2016, which forecasted a 6% increase in the number of welding professionals in the next 10 years [4]. In 2010, welders were hired at 61% by industrial manufacturing, at 11% for construction, at 5% for wholesale trade, and at 5% for maintenance and repair [5].

Welding fumes (WF) are a complex and heterogeneous mixture of fine (<2.5 µm) and ultrafine (<100 nm) particles made of metals and metallic oxides suspended in air and gases [1]. The particulate phase of WF is formed at the arc, at very high temperature (several thousand °C) compared to metals melting points, inducing vaporization of a fraction of the liquid metal bath. This is followed by a condensation mechanism under super-saturated conditions and a rapid growth of the condensed particles oxidizing upon contact with air (O_2, O_3, and NO_x) to form small particles of different complexes of metal oxides [6–8].

The chemical composition and emission rate of WF depend on several parameters. Some of them are related to each other. That includes the welding process (e.g., gas metal arc welding, shielded metal arc welding, and flux-cored arc welding), the diameter and composition of the wire or electrode (flux coating or flux-cored), the flow rate and composition of the shielding gas, and the presence of coatings on the welding materials (such as metals, paints, and solvent) [8,9]. The transition metals most frequently found in welding fumes are, in descending order, iron (Fe), manganese (Mn), chromium (Cr), nickel (Ni), copper (Cu), and zinc (Zn) [10,11].

Exposure levels to WF are variable and depend on the welding process and materials. The concentration of WF dust in the workplace can reach several tens of mg m^{-3} [12]. For instance, WF concentrations collected directly above the arc have been estimated in the range of 100–400 mg m^{-3} [13].

Several studies have shown that the inhalation of WF, after long-term exposure to severe fume levels (e.g., median value of 221 mg m^{-3} per year) [14], has adverse health effects, notably inducing an increase in respiratory and cardiovascular mortality and morbidity [10,14–17]. In 2018, WF were classified as group 1 carcinogens for human lungs by the International Agency for Research on Cancer [2]. However, only a few countries do have an occupational exposure limit (OEL) for total WF, although OELs exist for several constituents of WF [18]. In France, as in many other countries, the time-weighted average OEL value over 8 h (OEL-8 h) for total WF is limited to 5 mg m^{-3} in the breathing zone of the worker [12,19,20]. Depending on the composition of WF, the OEL-8h for the major WF constituents (Al, Ba, Be, Cd, Cr, Cu, Ti, Fe, Mn, Ni, Pb, V, and Zn) may also apply (Table A1 in Appendix A).

Inhaled ultrafine particles containing metals can be partially deposited along the respiratory tract and deeper in the pulmonary alveoli, where the macrophagic clearance mechanisms are slow [21]. Their small size allows for a large contact surface area with the physiological fluids covering the respiratory system, thus favoring their partial dissolution. Metals can participate in reactions triggering oxidative stress by inducing or promoting the formation of reactive oxygen species (ROS) [22–24]. In the pulmonary alveoli region, ROS can react quickly, with epithelial cells inducing damages and causing a cascade of local and systemic responses [25], leading notably to the development of acute and/or chronic heart and lung disease [26].

Given the importance of the ROS generation stage in mechanisms of particle toxicity [27], various in vivo and in vitro methods have been developed to evaluate the oxidizing properties of aerosols, i.e., their ROS formation potential, generally applied to atmospheric particles. Some tests are based on biological samples, such as the analysis of oxidative stress biomarkers in human bronchoalveolar lavage extracts, blood, or urine [10,17,28–31] or based on in vivo methods with animals testing. These tests are rather long, costly and difficult to carry out and present complications in making correlations between animal and human models (effect specificity, sensitivity, etc.) or can pose ethical problems. Toxicological tests on human cells of the respiratory system are also feasible in vitro but are complex, method-dependent, and time-consuming [32,33]. In comparison, as a first evaluation, chemical acellular in vitro tests are relatively simple to implement, easily reproducible, inexpensive, and fast. Some chemical tests are performed by direct measurement of ROS (e.g., $^{\bullet}OH$, HOOH, and $^{\bullet}O_2^-$) by spectroscopy spin trapping or by spin electronic resonance and fluorescence [34]. Other assays employ chemical cell-free tests based on the capacity of particles to oxidize target antioxidants chosen to mimic the constituents

of the respiratory tract lining fluids, which is the first physical interface encountered by inhaled substances [35,36]. These tests rely, for the most part, on analysis of the extracts of ambient particles collected on filters in the field for a specific period of time [27,37–43]. Among the most operated chemical cell-free tests, some are performed by measuring the loss rate of antioxidants such as ascorbic acid (AA) and glutathione (GSH) or a proxy of cellular reductants like dithiothreitol (DTT). Others are done using fluorescent probe as the diacetate 2′,7′-dichlorofluorescein (DCFH) assay [44,45]. These tests differ notably by their operating conditions and their sensitivity to some chemical compounds. Characteristics of the different cell-free tests are given in Table A2 of Appendix A. AA is very sensitive to Cu and Mn [31,36,46], while DCFH reacts significantly with H_2O_2 and transition metals [47–49]. DTT is the most sensitive to soluble transition metals [36,38,41,50] and some organic compounds such as Polycyclic Aromatic Hydrocarbon (PAHs) and quinones [51–56].

Although a previous work assessing the population-level impact of measured daily ambient oxidative potential (OP) from ambient air did not show significant health effects [57], DTT was correlated with health outcomes and with biological tests [44,58–61], confirming the need for more research on that matter. DTT-based chemical reactivity is considered a quantitative probe for assessing the capacity of particulate matter to catalyze ROS generation that will result in induction of oxidative stress at the cellular level [51,62]. DTT was notably correlated by the study of [27] with the production of H_2O_2.

The DTT method is performed in a two-step reaction. In the first step, the redox active chemicals present in the particles oxidize the dithiol function of DTT and form a DTT-disulfide, which is proportional to the concentration of ROS in the sample [51]. In the second step, the remaining dithiol (DTT in excess) reacts with Ellman's reagent (5,5′-dithiobis-2-nitrobenzoic acid or DTNB) and produces DTT-disulfide and a yellow chromophore (5-mercapto-2-nitrobenzoic acid or TNB), of which the absorbance is measured at 412 nm by visible spectrophotometry. The absorbance of TNB is directly proportional to the amount of DTT remaining in solution after its reaction with the particles [63]. This method is based on measurement of the linear rate of DTT consumption to determine the oxidative potential of the particles [38,51].

Several studies have suggested that the solubility of particulate metals in pulmonary fluids under physiological-like conditions (37 °C, pH 7.4), i.e., their bioaccessibility, is a key criterion for toxicological assessments [64–68]. In addition, the ROS generation caused by inhalation of particulate metals have been shown to play a major role in pulmonary toxicity and it can be evaluated by measurement of the oxidative potential [10,23,24,29,33,69,70]. The main question remaining to be fully understood is which metallic species are the most soluble contributors to oxidative potential. Regarding the particulate insoluble fraction not discussed in this study, Sauvain and Rossi [71] evidenced that functional groups on carbon nanoparticle surfaces could reversibly change their oxidation state, confirming their catalytic nature and explaining their ability to generate reactive oxygen species. Likewise, Leclercq et al. [72] demonstrated that the insoluble fraction of urban airborne fine particles ($PM_{2.5}$) could induce cytotoxicity while both soluble and insoluble particulate fractions could be linked to the secretion of cytokines.

The objective of this work is to assess the role of the main soluble transition metal constituents of WF (Cr, Cu, Fe, Mn, Ni, and Zn) and likely to participate in redox processes, with respect to the oxidative potential generated. These specific transition metals were selected as these elements constitute 92.4% and 88.5% in terms of oxide fractions of the total mass of the stainless steel and mild steel WF, respectively. These metals are generally found in WF in the valence states (+II) for Cu, Ni, and Zn; (+II and +III) for Fe; (+II, +III, and +IV) for Mn; and (+III and +VI) for Cr [73,74]. As far as we know, there are only two types of certified reference materials (CRMs) for WF commercially available: stainless steel (SSWF-1) and mild steel (MSWF-1) welding fumes. One WF CRM only certified for its chromium content exists although it is too expensive for routine uses [75]. In this study, we used a method of extraction and analysis of the fraction of transition metals of SSWF-1

and MSWF-1 soluble in a phosphate buffer solution (PB-soluble) under specific conditions (detailed in Sections 2.4 and 2.6), adapted from Caboche et al. [68]. This PB-soluble fraction is considered a proxy of the metal bioaccessibility (see Section 2.6). We also developed a method of evaluation of their DTT oxidative potential using a semiautomated chemical assay adapted from previous studies [38,40,50,51,68]. The same DTT analyses were carried out on selected metal salts for the main oxidation states of metals to decipher the OP^{DTT} contribution of each element.

2. Materials and Methods

2.1. Welding Fume-Certified Reference Materials

The total elemental mass fractions of the two certified reference materials (CRMs) of welding fumes, stainless steel (SSWF-1) and mild steel (MSWF-1), are reported in Table A3 of Appendix A. These materials from the Health and Safety Executive (HSE, UK) produced in 2012 were collected from ventilation ducts located above robotic welding stations in a car assembly plant and were subsequently processed in the laboratory [75]. The particles in both CRMs are smaller than 200 µm and form homogeneous finely divided particulate powders. WF CRMs are stored in brown glass vials away from light and moisture. According to the HSE certificate, the X-ray diffraction analysis (XRD) showed that MSWF-1 contained mainly major crystalline phases (Fe_3O_4, ZnO, and graphitic carbon) and a minor one (MnO). SSWF-1 showed spinel-type crystalline phases, such as Fe_3O_4, $Fe_3Mn_3O_8$, Mn_3O_4, and $FeCr_2O_4$. Nickel can be present in the form of mixed spinel oxides such as Fe_2NiO_4, $(Ni, Cr, Fe)_3O_4$, and Cr_2NiO_4 [9,75].

2.2. Phosphate Buffer Preparation

The PB solution was prepared at a total phosphate concentration of 0.1 mol L^{-1} made of 0.02 mol L^{-1} KH_2PO_4 (99%, Sigma Aldrich, St. Louis, MO, USA) and 0.08 mol L^{-1} K_2HPO_4 (98%, Sigma Aldrich) in ultrapure water (Milli-Q®, Millipore, Merck KGaA, Darmstadt, Germany) to reach a pH of 7.4 ± 0.1.

2.3. Metal Salts Preparation

Cu ($CuSO_4$ 99.8%, VWR International, Radnor, PA, USA), Mn ($Mn(NO_3)_2$ 97%, Sigma Aldrich), Ni ($NiCl_2$ 98%, Pomeac), and Zn ($ZnSO_4$ 99.5%, Fluka, Charlotte, NC, USA) metals were studied in the oxidation state (II), while Fe and Cr were studied in the oxidation states (III) ($FeCl_3$ 99%, Sigma Aldrich) and (VI) (CrO_3 98%, Sigma Aldrich), respectively. Cr (III) was not considered because it precipitates at pH > 6 to form the stable specie $Cr(OH)_3$ (s) [76]. Metal salts were dissolved in the PB to prepare stock solutions (3×10^{-4} mol L^{-1}) from which reagents with targeted concentrations were prepared through dilution with the PB solution before the experiments. The positive control 9,10-PQN (9,10-phenanthraquinone 99%, Sigma Aldrich) was prepared as a stock solution (5.1×10^{-4} mol L^{-1}) in absolute methanol (Biosolve, Biosolve Chimie, France) under a hood and stored in the freezer at −20 °C. An intermediate solution of 9,10-PQN (1.5×10^{-7} mol L^{-1}) diluted in absolute methanol was prepared the day of the experiment. PB (0.1 mol L^{-1}) and absolute methanol were used as negative controls.

2.4. Extraction of Metals from WF CRMs

A mass of 1 ± 0.1 mg of each WF CRM was placed in a 50-mL Teflon® FEP centrifuge tube to carry out the soluble metal extraction. PB was added considering a constant S/L ratio of 1/10,000 (g mL^{-1}) to avoid any competition or saturation phenomenon [68,77]. Samples were stirred transversely at a temperature of 37 °C in a water bath for 24 h. The 24-hour exposure is a "standard" duration allowing quantitative extraction of most metals, close to the residence time of particles in the lungs, which often leads to satisfactory correlations between metal dissolution and acute toxicity [73]. The samples were then centrifuged at 14,300 rpm for 15 min at 4 °C. The supernatant was filtered through a nylon syringe filter with a 0.22-µm porosity (Millipore®, Merck KGaA, Darmstadt, Germany) to

remove any remaining suspended fine particles. This extract was divided in two samples of 5 mL each. One was acidified with HNO_3 (67%, ultrapure, VWR international) to 0.1% v/v for subsequent analysis of the soluble metal concentrations by ICP-MS. The second one was stored as is at −20 °C to perform OP^{DTT} analysis later on.

2.5. Total Mineralization of WF

Mineralization before ICP-MS analyses was carried out in triplicate by a microwave digestion system (Ultrawave Milestone®, Sorisole, Italy, P = 40 bars, T_{max} = 220 °C, 70 min) in a mixture of HNO_3 (67%), H_2O_2 (30%) and HF (40%) (ultrapure, Sigma Aldrich) on a mass of 1 ± 0.1 mg of each WF CRM placed in Teflon tubes. The digests were diluted in 50 mL of ultrapure water and analyzed by ICP-MS (NeXion 300X, Perkin Elmer, Waltham, MA, USA) using the DRC™ mode with hydrogen. Repeated measurements were performed on acid blanks (n = 30), multielement quality control standard solutions (n = 6), digests of standard reference material (NIST SRM 1648a, n = 4), and each WF CRM (n = 9). The conditions of the ICP-MS analysis are given in Table A4 in Appendix A.

2.6. Determination of the Metal PB Solubility

In this study, the PB-soluble concentration of a metal was determined by ICP-MS analysis as the concentration of metal in the extract obtained after dissolution of the particulate sample in a potassium phosphate buffer solution under physiological-like conditions of temperature (37 °C), pH neutrality (pH 7.4), extraction time (24 h), and solid-to-liquid ratio (Section 2.4). This defined PB-soluble concentration is considered here in this study as an approximation of the metal bioaccessibility. Hence, the metal bioaccessibility, given in percentage, was calculated as the ratio of the PB-soluble ("bioaccessible") concentration of a given metal to its total concentration (see Section 2.5).

The choice of a simplified medium (PB), instead of a more complex physiological fluid, such as artificial simulated lung lining fluids (Gamble [68] or Hatch [11,78] solutions), is to restrict the role of ligands to only few species (oxo/hydroxo complexes, phosphates, and DTT sulfidic groups) in order to understand the oxidative action of metals.

2.7. DTT Method

On the day of the experiment, DTT (Cleland reagent, 1,4-dithiothreitol, Roche Diagnostics GmbH, Hong Kong, China) and DTNB (Ellman reagent, 5,5′-dithiobis-2-nitrobenzoic acid 99%, Sigma Aldrich) solutions were prepared in PB at concentrations of 300 µmol L^{-1} and 420 µmol L^{-1}, respectively. Solutions were kept in an ice bath in the dark during the experiment and were used within 24 h after preparation.

A semiautomated method was used for the DTT test [38,39,50,79] with a Spark 10M microplate reader (TECAN) and 96-well UV-transparent microplates (UV-Star®, Greiner Bio-One, Kremsmunster, Austria).

The total volume of the reaction mixture in a well was 300 µL. The DTT consumption was monitored every 10 min for 30 min during a three-step procedure. First, 100 µL of each sample (negative controls, positive control, WF extracts, and mono-elemental samples) were injected manually with a micropipette in the wells in quadruplicates. In the second step (DTT oxidation), 100 µL of DTT (300 µmol L^{-1}) was injected by an automated injector into each well. The mixture was incubated at 37 °C and automatically shaken for 3 seconds after DTT injection and every 5 min by linear stirring (1440 rpm) by the microplate reader. In the third step (reaction of the non-oxidized DTT with DTNB), DTT was quantified by adding 100 µL DTNB (420 µmol L^{-1}), which reacts quantitatively with DTT in excess to form the chromophore 2-nitro-5-thiobenzoic acid (TNB) instantly. After injection of DTNB, a 5-second agitation was carried out followed by the direct measurement of the absorption of TNB at a wavelength of 412 nm after 10, 20, and 30 min of reaction between DTT and the samples. Absorbance measurements were validated if the coefficient of variation between the quadruplicates was less than 5%. The measurements were carried out on the soluble metal salts and on the WF CRMs PB extracts.

The DTT consumption rate (μmol DTT L^{-1} min^{-1}) is the variation in the amount of DTT consumed as a function of time. The rate was determined from the initial slope (least square regression) of the absorbance curve of the TNB as a function of time. Absorbance was converted to DTT concentrations through the calibration curve formed by TNB absorbance as a function of DTT concentrations. The same procedure was applied to negative and positive controls.

The DTT intrinsic oxidative potential (OP^{DTT}) of the tested sample was defined as the difference between the DTT consumption rate of the sample extract in PB and the DTT consumption rate of the PB (negative control), expressed in μmol DTT $L^{-1}min^{-1}$ (Equation (1)).

$$OP^{DTT} = \text{DTT rate (Sample)} - \text{DTT rate (blank)}, \quad (1)$$

where DTT rate (Sample) is the variation in concentration of DTT over time in the presence of the sample extract in PB or in methanol for 9.10-PNQ and DTT rate (blank) is the variation of DTT concentration over time due to the blank. It corresponds to the background of DTT oxidation by atmospheric dissolved oxygen and to the presence of trace metal contaminant in the PB or methanol matrix.

The methodological detection limit (MDL) and quantification limit (MQL) of the OP^{DTT} measurement were calculated respectively as 3 and 10 times the standard deviation (σ) related to the average OP^{DTT} of 14 PB solutions (0.1 mol L^{-1}) carried out on different days. MDL and MQL were then determined as 0.024 μmol DTT L^{-1} min^{-1} and 0.081 μmol DTT L^{-1} min^{-1} respectively. In our setting, PB induces a negligible amount of DTT loss. OP^{DTT} measured for PB was 0.024 ± 0.008 μmol DTT L^{-1} min^{-1} in this study and 0.236 ± 0.082 μmol DTT L^{-1} min^{-1} in [38].

3. Results and Discussion

3.1. Total Elemental Contents in WF CRMs

An overview of the total elemental contents, PB-soluble concentrations, and fractions obtained for the major elements analyzed in the two WF CRMs tested (HSE MSWF-1 and SSWF-1) is given in Table 1. The total elemental contents are consistent with those of the certificated values of WF CRMs with a relative discrepancy below 5% for Cr and Ni in both CRMs, for Cu in MSWF-1, and for Fe in SSWF-1 and between 10 and 17% for Fe, Mn, and Zn in MSWF-1 and for Cu and Mn in SSWF-1. The small mass of WF CRMs (1 mg) used in this study compared to the recommended mass by the HSE certificate (10 mg) may induce errors due to heterogeneity of the CRM and weighing causing differences for some metals with certified values. MSWF-1 was mainly composed of Fe, Zn, and Mn (39–45%, 21–24%, and 1–2%, respectively) and contains small amounts of Cr, Cu, and Ni (<0.5%). SSWF-1 was mainly composed of Fe, Mn, Cr, and Ni (approximately 27–32%, 19–23%, 8–9%, and 3–4%, respectively) and contains low amounts of Cu and Zn (<0.5%). Both WF CRMs have a different proportion of transition metals. These different chemical compositions were consistent with the different filler materials used during the welding process, either mild steel or stainless steel (enriched in Ni and Cr). These WF CRMs contain other minor elements with uncertified total concentrations (except for Al, Ca, Pb, and Mg in MSWF-1), presented in an exhaustive elemental analysis given in Table A5 of Appendix A.

Table 1. Total content (μg g^{-1}), PB-soluble concentration (μg g^{-1}), and percentage of PB solubility obtained for the major elements analyzed in two welding fumes reference materials (stainless steel welding fumes (SSWF-1) and mild steel welding fumes (MSWF-1)) after 24-h extraction in PB (average ± σ, n = 9 replicates).

SSWF-1				
Element	**Ref. Value [1] (%)**	**Total Content [2] (μg g^{-1})**	**PB-soluble Concentration [3] (μg g^{-1})**	**PB Solubility [1] (%)**
Cr	8.40 ± 0.40	79,800 ± 4300	407 ± 34	0.51 ± 0.05
Cu	0.40 ± 0.12	4050 ± 220	248 ± 38	5.95 ± 0.99
Fe	29.80 ± 0.90	327,000 ±17,000	554 ± 32	0.17 ± 0.01
Mn	22.90 ± 0.50	189,500 ± 10,900	15,900 ± 2100	8.39 ± 1.20
Ni	3.70 ± 0.20	35,100 ± 1900	747 ± 100	2.11 ± 0.31
Zn	0.27 ± 0.08	2324 ± 81	78 ± 36	3.43 ± 0.75
MSWF-1				
Element	**Ref. Value [1] (%)**	**Total Content [2] (μg g^{-1})**	**PB-soluble Concentration [3] (μg g^{-1})**	**PB Solubility [1] (%)**
Cr	0.04 ± 0.01	338 ± 9	1.51 ± 0.50	0.70 ± 0.31
Cu	0.27 ± 0.03	2508 ± 84	274 ± 27	10.93 ± 1.09
Fe	42.80 ± 0.70	451,600 ± 7200	18 ± 10	0.03 ± 0.06
Mn	1.48 ± 0.03	13,070 ± 460	448 ± 69	3.42 ± 0.58
Ni	0.01 ± N/A	96.70 ± 6.40	<LOD	N/A
Zn	21.70 ± 0.90	211,400 ± 7700	5570 ± 930	2.64 ± 0.48

<LOD: below the limit of detection; N/A: not available; [1] Weight percent; [2] After acid digestion; [3] In PB 0.1 mol L^{-1}, pH 7.4, 37 °C, S/L ratio 1 mg/10 mL.

3.2. PB Solubility of Transition Metals in WF CRMs

The total metal PB solubility (sum of PB solubility of the six major metals analyzed) was similar in both WF CRMs (19–21%). However, the individual elemental solubility may be quite variable (Table 1). Very low values (below 1%) were observed in both WF CRMs for Cr and Fe, which were almost insoluble in the PB. Higher solubilities were found for Zn (around 3%) in both WF CRMs, for Mn (around 3.4%) in MSWF-1, and for Ni (2%) in SSWF-1 (Ni not present in MSWF-1). The highest PB solubility was observed for Cu (6 and 11% for SSWF-1 and MSWF-1, respectively) and for Mn (9%) in SSWF-1. The results show that PB solubility may vary depending on the element and the sample considered, notably for Cu and Mn. Other factors may influence the solubility such as the particle size distribution in the WF CRMs, which is not available in the certificate.

Keane et al. [73] hypothesized that soluble metal ions of WF in biological media can change their valence state. In addition, these authors suggested that the solubility products of transition metal phosphates are generally low. In other words, the concentrations of soluble metal ions could be very low in a neutral pH PB solution, a statement consistent with the rather low range of PB solubility measured in this study (maximum of 11%). The total Fe content in MSWF-1 was 451,600 μg g^{-1}, about 35 times greater than that of Mn (13,070 μg g^{-1}), while the PB-soluble concentrations of Fe was almost 25 times less than the Mn one (Table 1). This confirms that solubility was not only related to the total content of the element but also to its physicochemical properties [80].

Relative metal PB solubility (Fe < Cr–Ni < Zn–Cu–Mn) shows a similar trend to those found by Berlinger et al. [81], who studied the Hatch solubility of WF (collected in shipyards and in a factory producing heavy machinery). The conditions of the Hatch protocol are given in Table A6 in Appendix A. While the two extracting solutions and the elemental composition of the WF studied were different, they found similar trends for the less soluble compounds Fe (<1%), Cr, and Ni (4–7%) and for the most soluble compounds Cu, Mn, and Zn (13–27%). Hatch's solution is a more complex medium that

showed higher solubility values than the results using PB [11]. This variability can be linked to a multitude of parameters including the nature of the extraction solution used (salinity, ionic strength, presence of complexing agent or competing species, etc.) and the implementation procedure (type of agitation, solid/liquid ratio, etc.) and to the operating parameters of welding (type of process, base and wire materials, shielding gas, fluxes, etc.), which will influence the physicochemical composition of the WF [73,82,83]. This confirms the importance of having a standardized protocol to study the pulmonary solubility to better compare results between the different assays [68].

The low PB solubility observed for Fe (<1%) was in agreement with what has been reported in other publications dealing with WF [11,28,81,84] which classified Fe as the least soluble element. These publications suggest that Fe in WF is not in the form of soluble salts but mainly in the form of oxides (hematite) or in metal phases of low solubility. In addition, in simulated physiologic media at pH = 7.4 such as PB, Gamble, or Hatch solutions, Fe can form iron hydroxides which are also poorly soluble. On the contrary, for Mn and Cu, a larger fraction was probably present as soluble compounds [81]. Cu can be present as more soluble compounds in MSWF-1 (11%) than in SSWF-1 (6%), but inversely, Mn has a lower PB solubility in MSWF-1 (3.4%) than in SSWF-1 (9%). Keane et al. [73] have shown that Mn found in WF can be present in multiple oxidation states and speciation in different proportions, which can affect its solubility. The solubility of Ni was less than 3% although Ni (II) salts are generally very soluble, suggesting that this element was contained in the form of oxides as NiO [81]. Similar hypotheses can be raised for Zn and Cr with predominant occurrences of these elements as oxides or in metal phases. In addition, in the presence of Fe (II), Cr (VI) can be reduced to insoluble Cr (III) species, which can reduce its overall PB solubility [85].

The difference in PB solubility observed between the metals studied can be due to the different types of bonds by which metal compounds are linked to the solid matrix [86]. According to several works [9,10,24,84,87], fumes are formed by the evaporation of metals mainly at the level of the electric arc. Metal vapors condense and oxidize on contact with air and form small particles of different metal oxide complexes of very low solubility. During welding, the arc temperature is between 2500 °C and 3000 °C. The boiling temperatures of the transition metals Zn, Ni, Mn, Cu, and Cr are between 906 °C and 2730 °C and are lower than that of Fe (3000 °C). The hypothesis is that Fe species condense first to form the core of the particles and are followed by the condensation of Cr and Ni species, then by the more volatile Cu, Mn, and Zn species that will be preferably localized on the surface of the freshly formed particles, as observed during various metallurgical processing [88–90]. This causes Cu, Mn, and Zn compounds to likely be more PB-soluble and therefore better dissolved than Fe, Cr, and Ni. According to Feng [91], the elements retained in the crystal lattice in the form of an internal mixture forming the core of the particle are almost insoluble compared to the ones present at the surface of the particles. Floros [9] suggested that stainless steel WF consist mainly of spinel-type oxides, in particular iron-based spinel oxides of general formula Fe_{3-x} $(Cr, Ni, Mn, Ti)_xO_4$. Cr (VI) was not found in spinels, but it can be stabilized by certain alkali cations (Na and K) as chromates in SSWF. NiO was only present in significant content in some fumes of nickel-based products. This suggests that speciation of these elements may be different in the two types of WF CRMs, in agreement with the XRD analysis of the WF CRMs detailed earlier (see Section 2.1).

3.3. OP^{DTT} of Individual Transition Metals

To identify which metallic compounds can contribute to DTT loss in WF CRMs, DTT consumption was measured in the presence of each of the main dissolved transition metals in WF CRMs at a given concentration. OP^{DTT} was determined as the initial speed of DTT consumption over time at a specified metal concentration. These measurements do not take into consideration the OP^{DTT} that may be due to anions of the metal salts (nitrates, sulfates, and chlorides) [92,93]. Table 2 shows the OP^{DTT} measured at 1 μmol L^{-1} of each individual transition metal. The equimolar screening shows that

transition metals exhibit various sensitivities towards the DTT assay. Thereby, the decreasing order of dissolved transition metals (at 1 μmol L^{-1}) with regards to their DTT activity is Mn (II) > Cu (II) > Ni (II) > Fe (III), Zn (II), Cr (VI), consistent with the results of [38], although the order is reversed for Cu (II) and Mn (II). It is also consistent with previous studies on OP^{DTT} of metal salts that found that the most pro-inflammatory metals were Cu followed by Mn, while Ni, Fe, and Zn generated weaker effects [94]. The DTT loss rates obtained in the present study are lower than those of [38,79,95]. OP^{DTT} measured for the positive control 9,10-PQN at a concentration of 0.05 mol L^{-1} is consistent with the outcomes of Lyu et al. [79] and of Charrier and Anastasio [38] as they used concentrations of 0.1 mol L^{-1} and 0.15 mol L^{-1}, respectively (Figure A1 of Appendix A). The differences in the OP^{DTT} are probably due to the variability of the operating protocols, the metal salt speciation, and the concentrations used in these studies (Table A7 and Figures A1 and A2 of Appendix A). A harmonized procedure to measure the OP^{DTT} is then needed to better compare the results from different studies.

Table 2. Experimental metal oxidative potential (OP^{DTT}) at 1 μmol L^{-1} and regression equations for the dithiothreitol (DTT) loss rate depending on the concentration of individual metal ions.

Species	Experimental OP^{DTT} (μmol DTT L^{-1} min^{-1}) [a]	Range of Concentrations Tested (μmol L^{-1})	Regression Equations [b]	R^2	n [c]
Cr (VI)	0.026 ± 0.003	0.6–20	$y = 0.0242 \times x^{0.7441}$	0.99	5
Cu (II)	0.207 ± 0.032	0.1–40	$y = 0.2221 \times x^{0.2759}$	0.96	9
Fe (III)	0.032 ± 0.001	0.1–2	$y = 0.0291 \times x^{0.3065}$	0.95	5
Mn (II)	0.312 ± 0.052	0.6–40	$y = 0.3377 \times x^{0.1016}$	0.93	6
Ni (II)	0.128 ± 0.023	0.8–4	$y = 0.1150 \times x^{1.1546}$	0.96	6
Zn (II)	0.026 ± 0.002	0.1–12	$y = 0.0278 \times x^{0.2551}$	0.62	10

[a] OP^{DTT} per 1 μmol L^{-1} of metal species; [b] For each equation, y represents the rate of DTT loss (μmol DTT L^{-1} min^{-1}) and x is the metal ion concentration (μmol L^{-1}) in the DTT solution; [c] Number of values used in the regression: for each concentration, two independent determinations of the DTT loss rate were made and the resulting average rate was used in the regression.

To explain the reactivity of transition metals with DTT, only redox reactions between metals and DTT was considered in a first approximation, and complex speciation of metals in PB at pH 7.4 was then involved in a second step (Figure 1). Therefore, the redox potentials of metals and DTT were calculated at pH 7.4 assuming that each transition metal was in the same valence state as that in the salt or oxide compound used for the experiments (Table A8 of Appendix A). Based on these redox potentials, Cr (VI), Cu (II), Fe (III), and Ni (II) could oxidize DTT by a direct redox reaction allowed by thermodynamics (Section 1 of Figure 1).

On the one hand, the experimental results (Table 2) show that the OP^{DTT} of Cr (VI), Cu (II), and Ni (II) are above the MDL at 1 μmol L^{-1}. Out of these metals, Cu (II) and Ni (II) show significant DTT loss rates of 0.207 and 0.128 μmol DTT L^{-1} min^{-1}, respectively. These consumptions are higher than the stoichiometry of the redox reactions between these transition metals and DTT; thus, Cu (II) and Ni (II) probably catalyze DTT oxidation [42,96,97]. Experimentally, the complexation of Ni (II) and DTT has been observed and could favor electron transfer between Ni (II) and DTT [98]. Kachur et al. [96] proposed that the formation of the Cu^{2+}–DTT complex could catalyze the oxidation of free DTT by the formation of an oxygen-bearing intermediate. According to these authors, Cu (II) probably accepts an electron from DTT to form Cu (I), which quickly gives an electron to dissolved oxygen to form the superoxide ($^{\bullet}O_2^-$) species and to reform Cu (II). Regarding Cr (VI), it does not show a catalytic effect, suggesting that it might be reduced by DTT into Cr (III) through a direct redox reaction inducing slight DTT consumption [99].

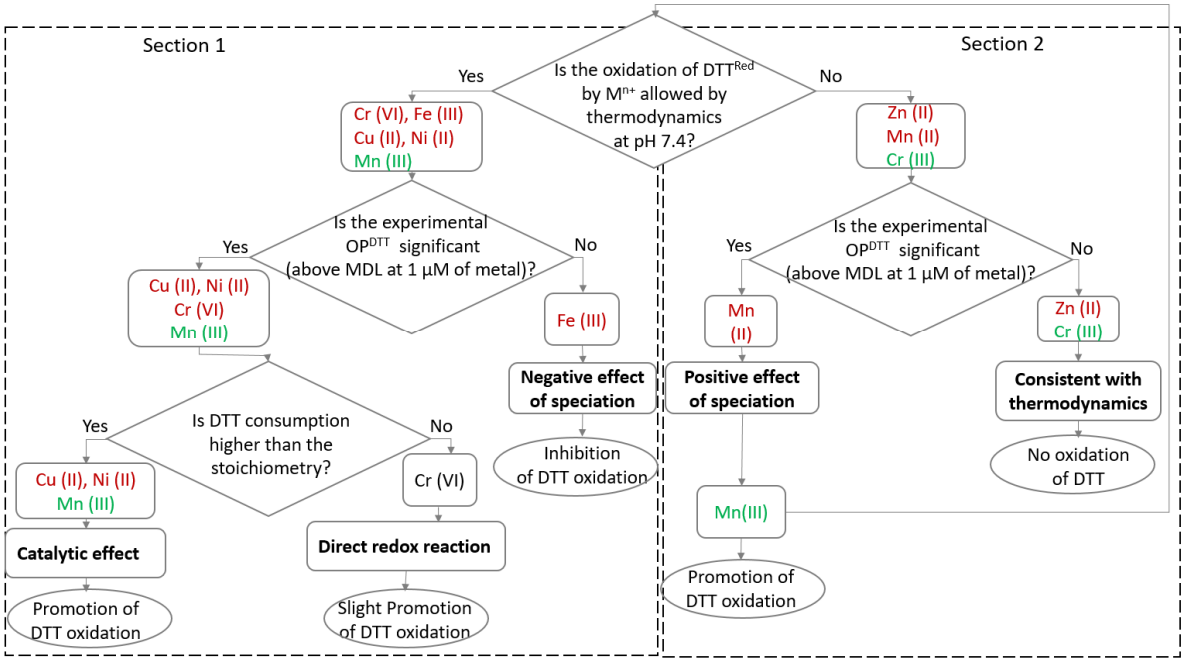

Figure 1. Flowchart of the suggested reactivity of transition metals with DTT: In red are the components initially present in the reactional media and in green are the components possibly resulting from a secondary reaction.

On the other hand, the OP^{DTT} measured for Fe (III) is below the MDL. This could be explained by the effect of speciation. According to the software Visual MINTEQ® 3.1 database [100] used to estimate the speciation of transition metals in PB, Fe^{3+} precipitates in water or PB to form hematite. Fe (III) could thus be unavailable to react with DTT, inducing inhibition of DTT oxidation and preventing the trigger of a Fenton-like oxidation [101,102].

With regard to Section 2 of Figure 1, thermodynamics do not allow the oxidation of DTT by Zn (II) or Mn (II). This can explain the OP^{DTT} close to the MDL found for Zn (II). On the contrary, the highest of all OP^{DTT} is found for Mn (II), suggesting that this metal is at least partly in a higher valence state. In fact, Mn^{2+} may be complexed or precipitated with PB constituents. It has been shown that these associations may enhance the formation and the stabilization of Mn (III) [103], which can thermodynamically oxidize DTT. Mn^{2+} could also be directly oxidized into Mn^{3+} by dissolved O_2 [104]. Thus, it can be assumed that manganese is possibly in a mixed Mn (II and III) valence state.

In a second approach, MINTEQ suggests that the divalent cations Cu^{2+}, Ni^{2+}, and Zn^{2+} are complexed by hydrogen phosphate (HPO_4^{2-}) to form neutral complexes such as $CuHPO_4$, $NiHPO_4$, and $ZnHPO_4$. The complexation determines the redox potential of the transition metal, generally by decreasing the oxidation capacity as electrons are trapped in metal–ligand bonds or covalent bonds. Interestingly, $CuHPO_4$ and $MnHPO_4$ have one unpaired electron. This could favor their oxidation potential (capacity to take electrons from DTT). For trivalent cations (Fe^{3+} and Cr^{3+}), MINTEQ suggests the complexation or precipitation with oxygen or hydroxide ions as $Cr(OH)_3$ or Fe_2O_3 (covalent bonds), consistent with what is suggested in Figure 1.

Moreover, the complexation of transition metals with DTT is theoretically possible (as suggested for Cu (II) and Ni (II) previously) although the DTT concentration is about 1000 times lower than the phosphates one. Unfortunately, DTT is not available in the MINTEQ database.

The mechanisms to explain the differences in OP^{DTT} for each metal are not yet fully understood, but some hypotheses can be made. Transition metals in PB may undergo different reactions influencing their speciation. They can form ions, or charged or neutral complexes, or they can precipitate. Thus, their speciation in various matrices may significantly influence the rates of DTT depletion.

3.4. Regression Equations of OP^{DTT}

To better understand the DTT assay responses, OP^{DTT} was measured as a function of different concentrations of selected individual transition metals. The choice of the concentration range tested was based on the PB-soluble concentrations of each metal (Figure A3 Appendix A) with at least 5 points well distributed over the chosen concentration range surrounding the target value.

The OP^{DTT} vs. molar concentration relationship (e.g., the dose–response relationship) was established for each metal via a power relationship (Figure A3 in Appendix A) that was used to calculate the regression equations compiled in Table 2.

OP^{DTT} of Fe (III) and Zn (II) are low across the concentration range tested compared to those of the other metals. Almost all their values are below the MQL (Section 2.7) which may induce a greater difference between the results and therefore more measurement uncertainty. In the case of Zn (II), it manifests itself by a low R^2 of 0.62. Cr (VI) shows a slight increase in DTT loss as a function of concentration above 5 µmol L^{-1} so its OP^{DTT} is higher than the MQL. The DTT losses induced by Mn (II), Cu (II), and Ni (II) are above the MQL for all concentration ranges tested. Over a certain concentration of Cu (II), Mn (II), and Ni (II), OP^{DTT} converges/tends to an asymptote. Previous studies [38,79,96,105] have also reported kinetics of OP^{DTT} with power relationships, suggesting that this shape may be due to the low efficiency of Mn (II) and Cu (II) to oxidize DTT at higher concentrations and to metal binding with the DTT. Regression equations obtained from kinetics may be used to tentatively predict OP^{DTT} induced by the WF CRMs in PB. This part is investigated in the next Section 3.5.

3.5. OP^{DTT} of Soluble Transition Metals from WF CRMs

To identify the redox-active species responsible for DTT loss in WF CRMs, OP^{DTT} was measured on the non-acidified PB CRMs extracts. Figure 2 shows that OP^{DTT} measured for PB extracts of SSWF-1 (0.484 $\pm$ 0.060 µmol L^{-1} DTT min^{-1}) is 2.2 times larger than the one measured for MSWF-1 (0.224 $\pm$ 0.033 µmol L^{-1} DTT min^{-1}). This difference can be explained by their respective compositions of transition metals. The total concentration of soluble metals (obtained by the sum of the concentrations of each dissolved metal) in extracts of SSWF-1 (41.4 µmol L^{-1}) is 4 times larger than that of MSWF-1 (11.8 µmol L^{-1}) due to the high Mn concentrations in SSWF-1 extract. Thus, the high OP^{DTT} in the SSWF-1 extract may be related to the soluble fractions of Mn (II), Cu (II), and Ni (II), which are more reactive towards DTT rather than the soluble fractions of Cr (VI), Zn (II), and Fe (III), which are less reactive. Zn is the most soluble compound in the extracts of MSWF-1 (10.2 µmol L^{-1}), but it is not very responsive to DTT (Table 2); the OP^{DTT} of MSWF-1 may thus be mostly linked to the soluble fractions of Mn (II) and Cu (II) (Table 1).

Simulated extracts (Figure 2) were prepared by mixing dissolved metal salts in PB at the same PB-soluble concentrations as in the MSWF-1 and SSWF-1 PB extracts. The OP^{DTT} measured for PB simulated extracts of SSWF-1 is 0.499 $\pm$ 0.013 µmol L^{-1} DTT min^{-1}, and the one measured for MSWF-1 is 0.220 $\pm$ 0.013 µmol L^{-1} DTT min^{-1}. The rates of DTT loss in the PB extracts of the two WF CRMs are similar (relative standard deviation of 3%) with those obtained for the mixtures simulating the soluble concentrations of the metals. This suggests that the selected metals used in the simulated extract are mainly responsible for OP^{DTT} in WF CRMs extracts. Thus, Mn (II) and Cu (II), the most soluble and the most reactive to DTT, respond similarly in both simulated and CRMs extracts.

OP^{DTT} induced by the WF CRMs are consistent with the results of [28], where SSWF induced more toxicity in the lungs than MSWF. In addition, Leonard et al. [106] have shown that the chemical composition of steel WF has a significant health impact related to the production of ROS, which was more important in the case of SSWF containing Mn and Ni in larger quantities compared to those of MSWF. Also, the outcomes of Verma et al [107] have shown that the production of ROS was correlated with transition metals, especially for Mn, Fe, and Cr.

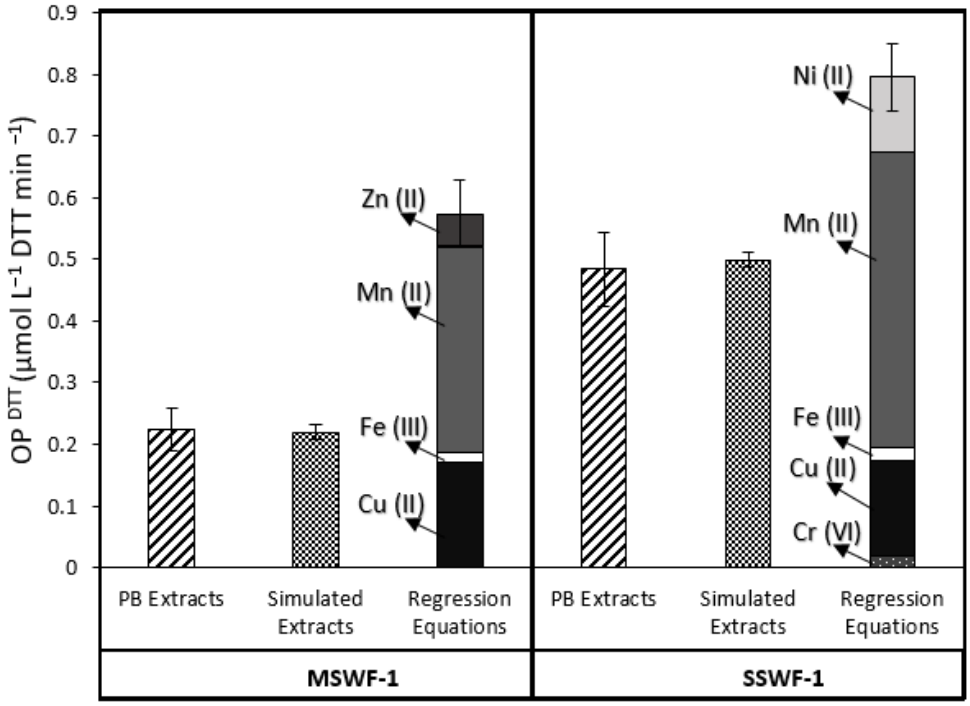

Figure 2. Blank-corrected rates of DTT loss (OP^{DTT}) in welding fume (WF) extracts of mild steel (MSWF) and stainless steel (SSWF) measured experimentally either on PB extracts (PB extracts; 6 replicates) or on reconstituted mixtures (Simulated Extracts; 3 replicates) and calculated theoretically via regression equations of the DTT loss rate as a function of the concentration of pure metals (Table 2).

OP^{DTT} from the regression fits of the experimental data (Figure 2) was calculated for SSWF-1 and for MSWF-1 by adding the regression-modelled DTT consumption rates obtained for each metal at its PB-soluble concentration, using the metal-specific regression equations (Table 2). Both calculated OP^{DTT} values from regression equations show a similar trend to the experimental ones (real PB and simulated extracts), with a higher DTT loss for SSWF-1 (0.796 ± 0.054 µmol L^{-1} DTT min^{-1}) than for MSWF-1 (0.573 ± 0.054 µmol L^{-1} DTT min^{-1}). However, the calculated values are higher than the PB extracts of WF CRMs by a factor of 1.6 for SSWF-1 and 2.5 for MSWF-1. This overestimation may be attributed in part to the combination of regression-modelling errors. In fact, as six regression equations were used to calculate the theoretical OP^{DTT} value, the combined error is at least approximately 2.5 ($\sqrt{6}$) times larger than the error of a single metal equation. Nevertheless, the main cause of overestimation of the calculated OP^{DTT} is likely to be linked to modifications in the speciation of various metals when mixed.

First, the complexation of metals with the different ligands present in solution (here, mainly phosphates and DTT) is a key factor influencing OP^{DTT} [108]. However, in these OP^{DTT} measurements, the ligand composition of the solution is the same for single metals and for the mixtures of metals (simulated and real PB extracts). Moreover, the possibility that the complexation of metals may be modified by a competition between different metals for the same ligands is unlikely. Indeed, the total phosphates concentration (0.1 mol L^{-1}) and DTT concentration (150 µmol L^{-1}) are always higher than the PB-soluble concentrations of metals (<40 µmol L^{-1}). Hence, the complexation of metals, although potentially a key factor, does not explain the difference between the OP^{DTT} of multi-metallic extracts and the calculated OP^{DTT} based on single-metal regression equations.

A second explanation is that the mix of metals may induce redox interactions between them, which are not considered by the theoretical calculation of individual elements. For example, Krawic and Zhitkovich [109] studied this effect by performing cellular tests in the presence of physiological antioxidants such as ascorbate and glutathione at pH 7.4. They showed that Fe (III) induced an antagonistic effect on the toxicity of Cr (VI) explained

by the reduction of Fe (III) in Fe (II) by a reducing agent and then the reduction of Cr (VI) by Fe (II) into the insoluble and less toxic Cr (III). In our study, one may assume that a redox interaction may occur between the two metals that mainly cause OP^{DTT}: Cu (II) and Mn (II). As explained in Section 3.3, the oxidation of DTT by Cu (II) produces Cu (I), which induces ROS generation and accelerates DTT consumption, while hydrogen phosphate favors the oxidation of Mn (II) to Mn (III), which oxidizes DTT. However, the standard reduction potential is 1.541 V for Mn (III)/Mn (II) and 0.153 V for Cu (II)/Cu (I), offering the possibility that Mn (III) oxidizes Cu (I), thus inhibiting the generation of ROS and limiting OP^{DTT} due to Cu (II). This reaction may be favored by the PB-soluble concentrations of Mn being always greater than Cu ones. Hence, the hypothesis is that the antagonistic effect on OP^{DTT} observed in multi-metallic mixtures is due to an indirect interaction between Mn (II) and Cu (II) through the generation of redox-active species Mn (III) and Cu (I).

4. Conclusions

Transition metals in the two WF CRMs (SSWF-1 and MSWF-1) mainly composed of Fe, Mn, Zn, Cu, Cr, and Ni in various proportions have shown different PB solubility. Cu and Mn were the most soluble elements in a phosphate buffer (PB) solution. Transition metals have also displayed different sensitivities toward DTT. Mn (II) and Cu (II) were found to be key elements of the OP^{DTT} of WF CRMs extracts. Mn (II), Cu (II), and Ni (II) might enhance DTT oxidation through redox catalytic mechanisms related to the formation of complexes with either phosphates or DTT. Moreover, regression equations obtained for each metal from the regression fitted to the experimental data have been tested to tentatively predict OP^{DTT} induced by the WF CRMs extracts in PB. Our findings showed that summing the main individual soluble metal DTT response induces a large overestimation probably linked to modifications in the speciation of various metals when mixed. The complexation of metals with the different ligands present in solution and the interaction between metals in the PB-soluble fraction are important phenomena that can influence OP^{DTT} depletion and therefore the potential health effect of inhaled WF. Further investigations are needed to understand the influence of the chemical composition of WF on their oxidative properties, notably by finely characterizing the metals speciation.

Author Contributions: Investigation and formal analysis, M.G.; writing—original draft preparation, M.G.; Writing—review and editing, and supervision, E.P., L.Y.A., D.R., and P.C.; All authors have read and agreed to the published version of the manuscript.

Funding: This research was funded by the Regional Council "Hauts-de-France", the Ministère de l'Enseignement Supérieur et de la Recherche, and the European Fund for Regional Economic Development (FEDER) through the CPER CLIMIBIO project, and by the French National Research Agency (ANR) through the PIA (Programme d'Investissement d'Avenir) under contract "ANR-11-LABX-0005-01" for the CaPPA project (Chemical and Physical Properties of the Atmosphere).

Institutional Review Board Statement: Not applicable.

Informed Consent Statement: Not applicable.

Data Availability Statement: The data presented in this study are available on request from the corresponding author.

Acknowledgments: We would like to thank Bruno Malet for performing the metal analyses and Nilmara de Oliveira Alves for contributing in the optimization of the DTT method.

Conflicts of Interest: The authors declare no conflict of interest.

Appendix A

Table A1. Occupational exposure limit values OEL-8 h and OEL-15 min applied in France of the main metals emitted during welding [12,20].

Metal	Form	OEL-8 h (mg m^{-3})	OEL-15 min (mg m^{-3})
Aluminum	Welding fumes	5	
Aluminum	Al_2O_3	10	
Baryum	Soluble compounds	0.5	
Beryllium	Beryllium compounds	0.002	
Cadmium	Oxides		0.05
Chromium	Chrome (VI)	0.001	0.005
Copper	Fumes	0.2	
Iron	Fe_2O_3 and fumes	5	
Lead	Metallic and Lead compounds	0.1	
Manganese	Mn_3O_4 and fumes	1	
Nickel	Oxide and trioxide	1	
Titanium	Titanium dioxide	10	
Vanadium		0.05	
Zinc	Oxide and fumes	5	

Table A2. Characteristics of the different cell-free tests to determine the oxidative potential of particles.

Test	Principles and Common Units	Detection	Sensitivity to	References
AA	O_2 consumption rate (nmol min^{-1} mg^{-1})	Clark electrode	Transition metals (Cu, Mn)	[31,40,46]
	AA consumption rate (nmol AA min^{-1} μg^{-1})	UV absorbance at 265 nm		
DTT	DTT consumption rate (nmol of DTT min^{-1} μg^{-1})	Vis absorbance at 412 nm	Organic compounds (PAHs and quinones) Transition metals (Cu, Zn, Cr, Fe, Ni, Mn)	[38,39,51]
DCFH	DCF production rate (nmol H_2O_2 min^{-1} μg^{-1})	Excitation at 485 nm Emission at 535 nm	ROS (H_2O_2) (ZnO, NiO, Ag) on the surface of ultrafine particles	[47–49]

Table A3. Mass fraction (% m/m) for analytes in the Health and Safety Executive (HSE) SSWF-1 and MSWF-1 adapted from [110,111].

SSWF-1							
Analyte	n	Certified Value			Indicative Value		
		% m/m			% m/m		
Chromium	7	8.40	±	0.40			
Copper	10				0.40	±	0.12
Iron	9	29.80	±	0.90			
Manganese	7	22.90	±	0.50			
Nickel	10	3.70	±	0.20			
Zinc	9				0.27	±	0.08

Table A3. *Cont.*

Analyte	n	MSWF-1					
		Certified Value			Indicative Value		
		% m/m			% m/m		
Aluminum	1				0.42		
Calcium	1				0.85		
Chromium	3				0.04	±	0.01
Copper	11				0.27	±	0.03
Iron	6	42.80	±	0.70			
Lead	1				0.005		
Magnesium	1				0.08		
Manganese	10	1.48	±	0.03			
Nickel	2				0.01		
Zinc	9	21.70	±	0.90			

n: number of data sets accepted.

Table A4. Conditions of the ICP-MS (NexION® 300) analysis.

Parameter	Setting
Introduction system	Conventional, Sapphire injector (1.5 mm), PFA-ST microflow nebulizer, PFA cyclonic spray chamber (7 mm baffle), Peltier cooler (+2 °C/−5 °C)
Mode	Dynamic reaction cell (DRC), reaction gas H_2 (2.5 mL min^{-1}), Plasma 1250 W, HNO_3 (2%), 20 sweeps
Internal standard	^{69}Ga, ^{103}Rh (1 µg L^{-1})
Quality control (QC)	Multi elementary solution (400 ng L^{-1})

Table A5. Total content (µg g^{-1}), PB-soluble concentration (µg g^{-1}), and PB solubility (%) obtained for all the elements analyzed in two welding fume reference materials (SSWF-1 and MSWF-1) after 24-h extraction in PB (average ± σ, n = 9 replicates).

Element	LOD Total Content [1] (µg g^{-1})	Total Content [1] (µg g^{-1})		LOD in PB [2] (µg g^{-1})	PB-soluble Concentration in PB [2] (µg g^{-1})		PB-soluble Fraction [3] (%)	
		MSWF	SSWF		MSWF	SSWF	MSWF	SSWF
Ag	10	31 ± 1	30.51 ± 0.44	0.05	2.17 ± 0.24	2.18 ± 0.41	7.00 ± 0.63	7.30 ± 0.95
Al	100	3850 ± 60	2080 ± 340	0.67	48 ± 19	15 ± 7	1.24 ± 0.31	0.71 ± 0.10
As	0.69	15 ± 1	84 ± 9	0.08	6.70 ± 1.50	14 ± 2	45 ± 10	17 ± 3
B	130	299 ± 11	299.26 ± 0.23	0.20	29 ± 11	35 ± 13	9.8 ± 4.2	11 ± 5
Ba	2.30	413 ± 30	33 ± 1	0.27	N/A	N/A	N/A	N/A
Be	0.48	1.13 ± 0.04	1.10 ± 0.10	0.01	N/A	N/A	N/A	N/A
Bi	0.21	0.62 ± 0.02	2.34 ± 0.27	0.01	N/A	N/A	N/A	N/A
Cd	0.37	0.86 ± 0.03	0.84 ± 0.04	0.01	N/A	N/A	N/A	N/A
Ce	0.05	2 ± 1	0.20 ± 0.08	0.01	0.029 ± 0.01	0.03 ± 0.01	1.45 ± 0.11	14.47 ± 0.75
Co	0.34	16 ± 1	279 ± 15	0.01	0.51 ± 0.20	6.04 ± 0.66	3 ± 1	2.17 ± 0.25
Cr	1.40	338 ± 9	79,800 ± 4300	0.17	1.51 ± 0.50	407 ± 34	0.70 ± 0.31	0.50 ± 0.05
Cs	0.16	0.38 ± 0.01	0.38 ± 0.01	0.01	N/A	N/A	N/A	N/A

Table A5. *Cont.*

Element	LOD Total Content [1] (μg g^{-1})	Total Content [1] (μg g^{-1})		LOD in PB [2] (μg g^{-1})	PB-soluble Concentration in PB [2] (μg g^{-1})		PB-soluble Fraction [3] (%)	
		MSWF	SSWF		MSWF	SSWF	MSWF	SSWF
Cu	1.60	2508 ± 84	4050 ± 220	0.73	274 ± 27	248 ± 38	10.93 ± 1.09	5.95 ± 0.99
Fe	120	451,600 ± 7200	327,000 ± 17,000	0.37	18 ± 10	554 ± 32	0.03 ± 0.06	0.17 ± 0.01
Hg	13	51 ± 2	50.60 ± 0.52	0.19	N/A	N/A	N/A	N/A
K	430	3240 ± 330	1570 ± 990	1100	N/A	N/A	N/A	N/A
La	0.10	0.91 ± 0.36	0.30 ± 0.10	0.01	N/A	N/A	N/A	N/A
Li	0.73	3 ± 1	2.14 ± 0.04	0.01	1.00 ± 0.30	0.18 ± 0.21	33 ± 11	10 ± 11
Mg	140	3520 ± 150	2770 ± 340	6.50	170 ± 150	91 ± 42	4.80 ± 3.60	3.35 ± 0.73
Mn	7.10	13,070 ± 460	189,500 ± 10,900	0.39	448 ± 69	15,900 ± 2100	3.42 ± 0.58	8.39 ± 1.20
Mo	0.47	8 ± 4	891 ± 48	0.06	1.04 ± 0.42	368 ± 60	13 ± 6	41 ± 7
Na	83	1660 ± 710	880 ± 240	2.30	N/A	N/A	N/A	N/A
Ni	1.03	96.70 ± 6.40	35,100 ± 1900	0.02	<LOD	747 ± 100	N/A	2.11 ± 0.31
Pb	0.58	39 ± 1	31.00 ± 0.85	0.01	0.60 ± 0.40	0.52 ± 0.38	1.46 ± 1.04	2 ± 1
Pd	0.61	1.42 ± 0.10	1.42 ± 0.01	0.01	N/A	N/A	N/A	N/A
Pt	0.44	1.03 ± 0.04	1.02 ± 0.02	0.01	N/A	N/A	N/A	N/A
Rb	7.02	16 ± 1	16.26 ± 0.23	2.50	N/A	N/A	N/A	N/A
Sb	0.32	25 ± 2	42 ± 2	0.01	5 ± 2	7 ± 2	20 ± 9	15 ± 5
Se	10	29 ± 8	42 ± 5	0.20	N/A	N/A	N/A	N/A
Si	3000	28,500 ± 2800	33,300 ± 1600	4	16,000 ± 12,000	35,000 ± 38,000	N/A	N/A
Sn	2.50	32 ± 4	111 ± 5	0.01	N/A	N/A	N/A	N/A
Sr	0.15	47 ± 4	9 ± 1	0.1	1 ± 1	1 ± 1	2 ± 2	11 ± 12
Th	0.10	0.30 ± 0.10	0.24 ± 0.01	0.01	N/A	N/A	N/A	N/A
TI	1000	2.12 ± 0.25	0.30 ± 0.01	32	N/A	N/A	N/A	N/A
Ti	0.13	3528 ± 1100	3340 ± 980	0.10	640 ± 160	840 ± 240	18 ± 3	24 ± 4
U	0.10	0.24 ± 0.01	0.32 ± 0.13	0.01	N/A	N/A	N/A	N/A
V	0.47	5 ± 1	197 ± 9	0.01	0.47 ± 0.47	19 ± 2	9 ± 10	10 ± 1
W	15	34 ± 1	34.26 ± 0.22	0.78	N/A	N/A	N/A	N/A
Zn	10	211,400 ± 7700	2324 ± 81	0.32	5570 ± 930	78 ± 36	2.64 ± 0.48	3.43 ± 0.75

LOD: Limit of detection; N/A: Not available; [1] After acid digestion; [2] In PB 0.1 mol L^{-1}, pH 7.4, 37 °C, S/L ratio 1 mg/10 mL; [3] Weight percent.

Table A6. Experimental conditions to study the bioaccessibility of welding fumes in 10 mL of extracting solutions during 24 h at 37 °C.

Experimental Conditions and Bioaccessibility		This Study		Berlinger et al. [81]
Conditions	Dissolution media (pH) Quantity	Phosphate buffer (7.4) 1 mg		Hatch's solution (7.4) Filter
	Material Element	HSE-SSWF-1	HSE-MSWF-1	Mix of WF
Bioaccessibility (%)	Fe	0.17 ± 0.01	0.03 ± 0.06	<1
	Cr	0.51 ± 0.05	0.70 ± 0.31	4–6
	Ni	2.11 ± 0.31	N/A	4–6
	Zn	3.43 ± 0.75	2.64 ± 0.48	13–27
	Cu	5.95 ± 0.99	10.93 ± 1.09	13–27
	Mn	8.39 ± 1.20	3.42 ± 0.58	13–27

Table A7. Comparison of the OP^{DTT} method used in this study and in Charrier and Anastasio [38].

Conditions	Charrier and Anastasio [38]	This Study
Common conditions	100 µmol L^{-1} DTT in 0.1 mol L^{-1} phosphate buffer pH 7.4 37 °C DTNB in 0.1 mol L^{-1} phosphate buffer TNB absorbance measured at 412 nm	
Sample volume	<100 µL	100 µL
DTT volume	3000 µL Shaking table (speed 4)	100 µL 15 s shaking
Extra reagent	At a known time take 500 µL aliquot of reaction mixture 0.5 mL of 10% trichloracetic acid	/
DTNB volume	50 µL DTNB 10 mmol L^{-1} shaking	100 µL DTNB 140 µmol L^{-1} shaking (5 s)
DTT/DTNB reaction time	5 min	5 s
Extra reagent	2 mL of 0.4 mol L^{-1} Tris Base pH (8.9) 20 mmol L^{-1} EDTA	/

Table A8. List of redox potentials at T = 25 °C, P = 1 atm [112], pH 7.4.

Oxidant	Reducer	E° (V) pH 7.4 *
H_2O_2	H_2O	+1.776
Mn^{3+}	Mn^{2+}	+1.541
O_2	H_2O	+1.229
MnO_2	Mn^{2+}	+0.888
Fe^{3+}	Fe^{2+}	+0.771
CrO_4^{2-}	$Cr(OH)_3$	+0.519
Cu^{2+}	Cu	+0.342
Cu^{2+}	Cu^{+}	+0.153
Ni^{2+}	Ni	−0.257
DTT-oxidized	**DTT-reduced**	−0.330
Fe^{2+}	Fe	−0.447
Zn^{2+}	Zn	−0.762
$Cr(OH)_3$	Cr	−1.091
Mn^{2+}	Mn	−1.185

* The redox couples were classified in order of decreasing E° (V) at pH 7.4.

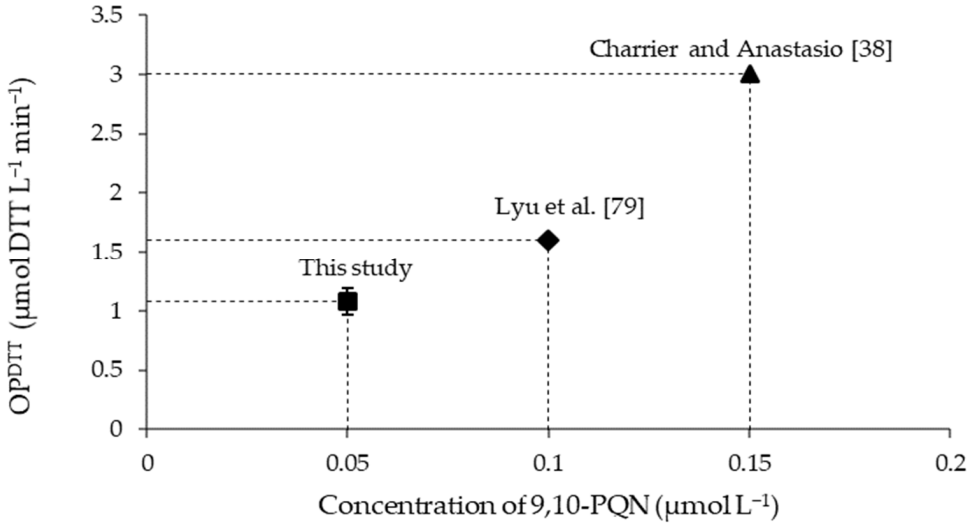

Figure A1. OP^{DTT} blank-corrected for 9,10-PQN used as a positive control: the concentration of 9,10-PQN is 0.05 μmol L^{-1} in this study, 0.1 μmol L^{-1} in Lyu et al. [79], and 0.15 μmol L^{-1} in Charrier and Anastasio [38].

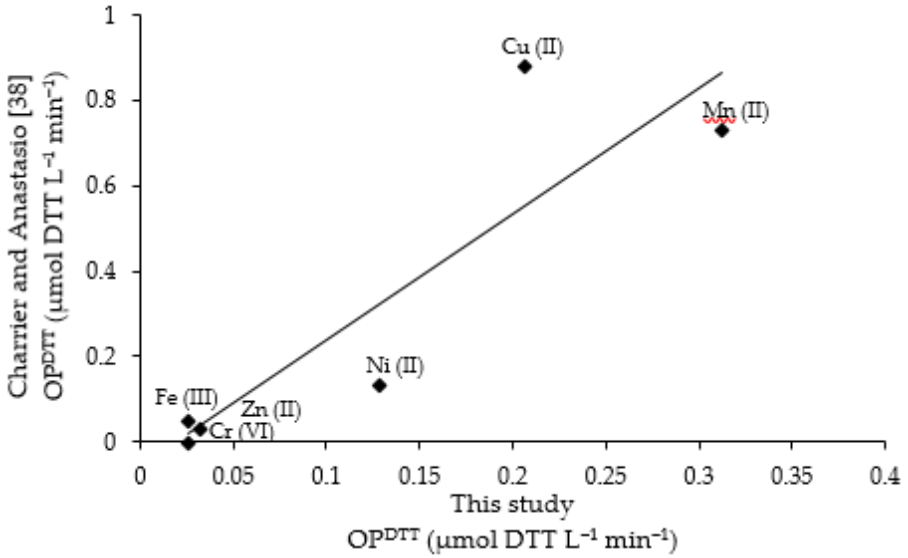

Figure A2. Scatter plot showing the positive correlation between OP^{DTT} (μmol DTT L^{-1} min^{-1}) measured in this study and in Charrier and Anastasio [38] for each metal at 1 μmol L^{-1} (in ascending order: Cr (VI), Zn (II), Fe (III), Ni (II), Cu (II), and Mn (II)).

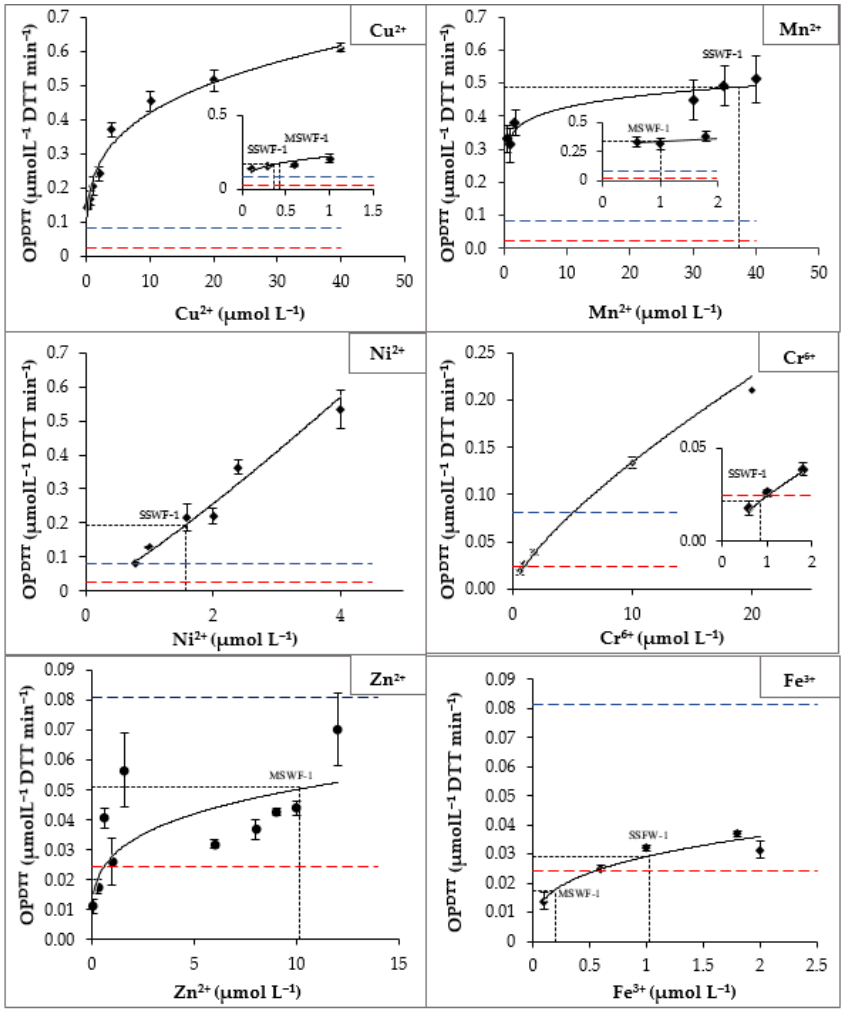

Figure A3. Blank-corrected rates of DTT loss as a function of the concentration of soluble metal for six DTT-reactive transition metals: each point represents the average (±σ) of multiple individual rate determinations. Circular points represent experimental OP measurement. Lines represent regression fits to the experimental data; the corresponding equations are listed in Table 2 of the manuscript. The red graduated lines denote the methodological detection limit (MDL), and the blue ones denote the methodological quantification limit (MQL) (defined in the Section 2.7 of the manuscript). SSWF-1 refers to stainless steel welding fume and MSWF-1 refers to mild steel welding fume PB-soluble concentration.

References

1. Antonini, J.M.; Lewis, A.B.; Roberts, J.R.; Whaley, D.A. Pulmonary effects of welding fumes: Review of worker and experimental animal studies. *Am. J. Ind. Med.* **2003**, *43*, 350–360. [CrossRef] [PubMed]
2. IARC. *Welding, Molybdenum Trioxide, and Indium Tin Oxide*; IARC Monograph Group on the Evaluation of Carcinogenic Risks to Humans: Lyon, France, 2018; Volume 118, ISBN 978-92-832-0156-4.
3. Cena, L.G.; Keane, M.J.; Chisholm, W.P.; Stone, S.; Harper, M.; Chen, B.T. A Novel Method for Assessing Respiratory Deposition of Welding Fume Nanoparticles. *J. Occup. Environ. Hyg.* **2014**, *11*, 771–780. [CrossRef] [PubMed]
4. Office of Labor Statistics Occupational Outlook Handbook. *Welders, Cutter, Solders, and Brazers*; U.S. Department of Labor: Washington, DC, USA, 2016.
5. Office of Labor Statistics Occupational Outlook Handbook Employment. *Welders, Cutter, Solders, and Brazers*; Department of Labor: Washington, DC, USA, 2012.
6. Zimmer, A.T.; Biswas, P. Characterization of the aerosols resulting from arc welding processes. *J. Aerosol Sci.* **2001**, *32*, 993–1008. [CrossRef]
7. Witschger, O.; Fabries, J.-F. Particules ultrafines et santé au travail—Caractéristiques et effets potentiels sur la santé. *Cah. Notes Doc.* **2005**, *15*, 21–35.
8. Berlinger, B.; Benker, N.; Weinbruch, S.; L'Vov, B.; Ebert, M.; Koch, W.; Ellingsen, D.G.; Thomassen, Y. Physicochemical characterisation of different welding aerosols. *Anal. Bioanal. Chem.* **2011**, *399*, 1773–1780. [CrossRef]

9. Floros, N. Welding fume main compounds and structure. *Weld. World* **2018**, *62*, 311–316. [CrossRef]
10. Antonini, J.M.; Clarke, R.W.; Krishna, M.G.G.; Sreekanthan, P.; Jenkins, N.; Eagar, T.W.; Brain, J.D. Freshly generated stainless steel welding fume induces greater lung inflammation in rats as compared to aged fume. *Toxicol. Lett.* **1998**, *98*, 77–86. [CrossRef]
11. Berlinger, B.; Ellingsen, D.G.; Náray, M.; Záray, G.; Thomassen, Y. A study of the bio-accessibility of welding fumes. *J. Environ. Monit.* **2008**, *10*, 1448. [CrossRef]
12. Ricaud, M. Fumées de Soudage Et Des Techniques Connexes. 2017. Available online: http://www.inrs.fr/media.html?refINRS=ED%206132 (accessed on 20 August 2019).
13. Ulfvarson, U. Survey of air contaminants from welding. *Scand. J. Work Environ. Health* **1981**, *7*, 1–28.
14. Buerke, U.; Schneider, J.; Rösler, J.; Woitowitz, H.-J. Interstitial pulmonary fibrosis after severe exposure to welding fumes. *Am. J. Ind. Med.* **2002**, *41*, 259–268. [CrossRef]
15. Antonini, J.M. Health Effects Associated with Welding. In *Comprehensive Materials Processing*; Elsevier: Amsterdam, The Netherlands, 2014; pp. 49–70, ISBN 978-0-08-096533-8.
16. Donaldson, K. Ultrafine particles. *Occup. Environ. Med.* **2001**, *58*, 211–216. [CrossRef] [PubMed]
17. Zeidler-Erdely, P.C.; Kashon, M.L.; Battelli, L.A.; Young, S.-H.; Erdely, A.; Roberts, J.R.; Reynolds, S.H.; Antonini, J.M. Pulmonary inflammation and tumor induction in lung tumor susceptible A/J and resistant C57BL/6J mice exposed to welding fume. *Part. Fibre Toxicol.* **2008**, *5*, 12. [CrossRef] [PubMed]
18. Harris, M. Welding fume is a Group 1 carcinogen with no OEL and no method—Suggestions for a path forward. *J. Occup. Environ. Hyg.* **2019**, *16*, 367–371. [CrossRef] [PubMed]
19. ACGIH. Welding fumes, not otherwise specified. In *Documentation of the Threshold Limit Values for Chemical Substances*; American Conference of Governmental Industrial Hygienists: Cincinnati, OH, USA, 2001; Volume 3, pp. 1726–1727.
20. GESTIS. GESTIS International Limit Values. Available online: https://limitvalue.ifa.dguv.de/ (accessed on 15 October 2020).
21. Oberdörster, G.; Maynard, A.; Donaldson, K.; Castranova, V.; Fitzpatrick, J.; Ausman, K.; Carter, J.; Karn, B.; Kreyling, W.; Lai, D.; et al. Principles for characterizing the potential human health effects from exposure to nanomaterials: Elements of a screening strategy. *Part. Fibre Toxicol.* **2005**, *2*, 8. [CrossRef]
22. Wilson, M.R.; Lightbody, J.H.; Donaldson, K.; Sales, J.; Stone, V. Interactions between ultrafine particles and transition metals in vivo and in vitro. *Toxicol. Appl. Pharmacol.* **2002**, *184*, 172–179. [CrossRef]
23. Graczyk, H.; Lewinski, N.; Zhao, J.; Sauvain, J.-J.; Suarez, G.; Wild, P.; Danuser, B.; Riediker, M. Increase in oxidative stress levels following welding fume inhalation: A controlled human exposure study. *Part. Fibre Toxicol.* **2015**, *13*, 31. [CrossRef]
24. Graczyk, H.; Lewinski, N.; Zhao, J.; Concha-Lozano, N.; Riediker, M. Characterization of Tungsten Inert Gas (TIG) Welding Fume Generated by Apprentice Welders. *Ann. Occup. Hyg.* **2016**, *60*, 205–219. [CrossRef]
25. Riediker, M. Cardiovascular Effects of Fine Particulate Matter Components in Highway Patrol Officers. *Inhal. Toxicol.* **2007**, *19* (Suppl. 1), 99–105. [CrossRef]
26. Newby, D.E.; Mannucci, P.M.; Tell, G.S.; Baccarelli, A.A.; Brook, R.D.; Donaldson, K.; Forastiere, F.; Franchini, M.; Franco, O.H.; Graham, I.; et al. Expert position paper on air pollution and cardiovascular disease. *Eur. Heart J.* **2015**, *36*, 83–93. [CrossRef]
27. Xiong, Q.; Yu, H.; Wang, R.; Wei, J.; Verma, V. Rethinking Dithiothreitol-Based Particulate Matter Oxidative Potential: Measuring Dithiothreitol Consumption versus Reactive Oxygen Species Generation. *Environ. Sci. Technol.* **2017**, *51*, 6507–6514. [CrossRef]
28. Antonini, J.; Lawryk, N.; Murthy, G.; Brain, J. Effect of welding fume solubility on lung macrophage viability and function in vitro. *J. Toxicol. Environ. Health A* **1999**, *58*, 343–363. [CrossRef] [PubMed]
29. Antonini, J.; Leonard, S.; Roberts, J.; Solano, L.C.; Young, S.-H.; Shi, X.; Taylor, M. Effect of stainless steel manual metal arc welding fume on free radical production, DNA damage, and apoptosis induction. *Mol. Cell. Biochem.* **2005**, *279*, 17–23. [CrossRef] [PubMed]
30. Mudway, I.S.; Stenfors, N.; Duggan, S.T.; Roxborough, H.; Zielinski, H.; Marklund, S.L.; Blomberg, A.; Frew, A.J.; Sandström, T.; Kelly, F.J. An in vitro and in vivo investigation of the effects of diesel exhaust on human airway lining fluid antioxidants. *Arch. Biochem. Biophys.* **2004**, *423*, 200–212. [CrossRef] [PubMed]
31. Stoeger, T.; Takenaka, S.; Frankenberger, B.; Ritter, B.; Karg, E.; Maier, K.; Schulz, H.; Schmid, O. Deducing in Vivo Toxicity of Combustion-Derived Nanoparticles from a Cell-Free Oxidative Potency Assay and Metabolic Activation of Organic Compounds. *Environ. Health Perspect.* **2009**, *117*, 54–60. [CrossRef] [PubMed]
32. Karlsson, H.L.; Gliga, A.R.; Calléja, F.M.; Gonçalves, C.S.; Wallinder, I.O.; Vrieling, H.; Fadeel, B.; Hendriks, G. Mechanism-based genotoxicity screening of metal oxide nanoparticles using the ToxTracker panel of reporter cell lines. *Part. Fibre Toxicol.* **2014**, *11*, 41. [CrossRef]
33. McCarrick, S.; Wei, Z.; Moelijker, N.; Derr, R.; Persson, K.-A.; Hendriks, G.; Wallinder, I.; Hedberg, Y.; Karlsson, H. High variability in toxicity of welding fume nanoparticles from stainless steel in lung cells and reporter cell lines: The role of particle reactivity and solubility. *Nanotoxicology* **2019**, *13*, 1293–1309. [CrossRef]
34. Janssen, N.A.H.; Yang, A.; Strak, M.; Steenhof, M.; Hellack, B.; Gerlofs-Nijland, M.E.; Kuhlbusch, T.; Kelly, F.; Harrison, R.; Brunekreef, B.; et al. Oxidative potential of particulate matter collected at sites with different source characteristics. *Sci. Total Environ.* **2014**, *472*, 572–581. [CrossRef]
35. Hedayat, F.; Stevanovic, S.; Miljevic, B.; Bottle, S.; Ristovski, Z.D. Review-evaluating the molecular assays for measuring the oxidative potential of particulate matter. *Chem. Ind. Chem. Eng. Q.* **2014**, *21*, 201–210. [CrossRef]

36. Visentin, M.; Pagnoni, A.; Sarti, E.; Pietrogrande, M.C. Urban PM2.5 oxidative potential: Importance of chemical species and comparison of two spectrophotometric cell-free assays. *Environ. Pollut.* **2016**, *219*, 72–79. [CrossRef]
37. Hung, H.-F.; Wang, C.-S. Experimental determination of reactive oxygen species in Taipei aerosols. *J. Aerosol Sci.* **2001**, *32*, 1201–1211. [CrossRef]
38. Charrier, J.G.; Anastasio, C. On dithiothreitol (DTT) as a measure of oxidative potential for ambient particles: Evidence for the importance of soluble transition metals. *Atmos. Chem. Phys. Print* **2012**, *12*, 11317–11350. [CrossRef]
39. Fang, T.; Verma, V.; Guo, H.; King, L.E.; Edgerton, E.S.; Weber, R.J. A semi-automated system for quantifying the oxidative potential of ambient particles in aqueous extracts using the dithiothreitol (DTT) assay: Results from the Southeastern Center for Air Pollution and Epidemiology (SCAPE). *Atmos. Meas. Tech.* **2015**, *8*, 471–482. [CrossRef]
40. Fang, T.; Verma, V.; Bates, J.T.; Abrams, J.; Klein, M.; Strickland, M.J.; Sarnat, S.E.; Chang, H.H.; Mulholland, J.A.; Tolbert, P.E.; et al. Oxidative potential of ambient water-soluble PM2.5; in the southeastern United States: Contrasts in sources and health associations between ascorbic acid (AA) and dithiothreitol (DTT) assays. *Atmos. Chem. Phys.* **2016**, *16*, 3865–3879. [CrossRef]
41. Verma, V.; Rico-Martinez, R.; Kotra, N.; King, L.; Liu, J.; Snell, T.W.; Weber, R.J. Contribution of Water-Soluble and Insoluble Components and Their Hydrophobic/Hydrophilic Subfractions to the Reactive Oxygen Species-Generating Potential of Fine Ambient Aerosols. *Environ. Sci. Technol.* **2012**, *46*, 11384–11392. [CrossRef]
42. Lin, M.; Yu, J.Z. Dithiothreitol (DTT) concentration effect and its implications on the applicability of DTT assay to evaluate the oxidative potential of atmospheric aerosol samples. *Environ. Pollut.* **2019**, *251*, 938–944. [CrossRef]
43. Massimi, L.; Ristorini, M.; Simonetti, G.; Frezzini, M.A.; Astolfi, M.L.; Canepari, S. Spatial mapping and size distribution of oxidative potential of particulate matter released by spatially disaggregated sources. *Environ. Pollut.* **2020**, *266*, 115271. [CrossRef]
44. Bates, J.T.; Fang, T.; Verma, V.; Zeng, L.; Weber, R.J.; Tolbert, P.E.; Abrams, J.Y.; Sarnat, S.E.; Klein, M.; Mulholland, J.A.; et al. Review of Acellular Assays of Ambient Particulate Matter Oxidative Potential: Methods and Relationships with Composition, Sources, and Health Effects. *Environ. Sci. Technol.* **2019**, *53*, 4003–4019. [CrossRef]
45. Pietrogrande, M.; Russo, M.; Zagatti, E. Review of PM Oxidative Potential Measured with Acellular Assays in Urban and Rural Sites across Italy. *Atmosphere* **2019**, *10*, 626. [CrossRef]
46. Di Stefano, E.; Eiguren-Fernandez, A.; Delfino, R.J.; Sioutas, C.; Froines, J.R.; Cho, A.K. Determination of metal-based hydroxyl radical generating capacity of ambient and diesel exhaust particles. *Inhal. Toxicol.* **2009**, *21*, 731–738. [CrossRef]
47. Venkatachari, P.; Hopke, P.K. Development and Laboratory Testing of an Automated Monitor for the Measurement of Atmospheric Particle-Bound Reactive Oxygen Species (ROS). *Aerosol Sci. Technol.* **2008**, *42*, 629–635. [CrossRef]
48. Sauvain, J.-J.; Rossi, M.J.; Riediker, M. Comparison of Three Acellular Tests for Assessing the Oxidation Potential of Nanomaterials. *Aerosol Sci. Technol.* **2013**, *47*, 218–227. [CrossRef]
49. King, L.E.; Weber, R.J. Development and testing of an online method to measure ambient fine particulate reactive oxygen species (ROS) based on the 2′,7′-dichlorofluorescin (DCFH) assay. *Atmos. Meas. Tech.* **2013**, *6*, 1647–1658. [CrossRef]
50. Calas, A.; Uzu, G.; Martins, J.M.F.; Voisin, D.; Spadini, L.; Lacroix, T.; Jaffrezo, J.-L. The importance of simulated lung fluid (SLF) extractions for a more relevant evaluation of the oxidative potential of particulate matter. *Sci. Rep.* **2017**, *7*, 11617. [CrossRef] [PubMed]
51. Cho, A.K.; Sioutas, C.; Miguel, A.H.; Kumagai, Y.; Schmitz, D.A.; Singh, M.; Eiguren-Fernandez, A.; Froines, J.R. Redox activity of airborne particulate matter at different sites in the Los Angeles Basin. *Environ. Res.* **2005**, *99*, 40–47. [CrossRef]
52. Chung, M.Y.; Lazaro, R.A.; Lim, D.; Jackson, J.; Lyon, J.; Rendulic, D.; Hasson, A.S. Aerosol-Borne Quinones and Reactive Oxygen Species Generation by Particulate Matter Extracts. *Environ. Sci. Technol.* **2006**, *40*, 4880–4886. [CrossRef]
53. Jiang, H.; Jang, M.; Sabo-Attwood, T.; Robinson, S.E. Oxidative potential of secondary organic aerosols produced from photooxidation of different hydrocarbons using outdoor chamber under ambient sunlight. *Atmos. Environ.* **2016**, *131*, 382–389. [CrossRef]
54. McWhinney, R.D.; Badali, K.; Liggio, J.; Li, S.-M.; Abbatt, J.P.D. Filterable Redox Cycling Activity: A Comparison between Diesel Exhaust Particles and Secondary Organic Aerosol Constituents. *Environ. Sci. Technol.* **2013**, *47*, 3362–3369. [CrossRef]
55. McWhinney, R.; Zhou, S.; Abbatt, J. Naphthalene SOA: Redox activity and naphthoquinone gas-particle partitioning. *Atmos. Chem. Phys.* **2013**, *13*, 9731–9744. [CrossRef]
56. Saffari, A.; Hasheminassab, S.; Shafer, M.M.; Schauer, J.J.; Chatila, T.A.; Sioutas, C. Nighttime aqueous-phase secondary organic aerosols in Los Angeles and its implication for fine particulate matter composition and oxidative potential. *Atmos. Environ.* **2016**, *133*, 112–122. [CrossRef]
57. Atkinson, R.W.; Samoli, E.; Analitis, A.; Fuller, G.W.; Green, D.C.; Anderson, H.R.; Purdie, E.; Dunster, C.; Aitlhadj, L.; Kelly, F.J.; et al. Short-term associations between particle oxidative potential and daily mortality and hospital admissions in London. *Int. J. Hyg. Environ. Health* **2016**, *219*, 566–572. [CrossRef]
58. Shiraiwa, M.; Ueda, K.; Pozzer, A.; Lammel, G.; Kampf, C.J.; Fushimi, A.; Enami, S.; Arangio, A.M.; Fröhlich-Nowoisky, J.; Fujitani, Y.; et al. Aerosol Health Effects from Molecular to Global Scales. *Environ. Sci. Technol.* **2017**, *51*, 13545–13567. [CrossRef] [PubMed]
59. Abrams, J.Y.; Weber, R.J.; Klein, M.; Samat, S.E.; Chang, H.H.; Strickland, M.J.; Verma, V.; Fang, T.; Bates, J.T.; Mulholland, J.A.; et al. Associations between Ambient Fine Particulate Oxidative Potential and Cardiorespiratory Emergency Department Visits. *Environ. Health Perspect.* **2017**, *125*, 107008. [CrossRef] [PubMed]

60. Costabile, F.; Gualtieri, M.; Canepari, S.; Tranfo, G.; Consales, C.; Grollino, M.G.; Paci, E.; Petralia, E.; Pigini, D.; Simonetti, G. Evidence of association between aerosol properties and in-vitro cellular oxidative response to PM1, oxidative potential of PM2.5, a biomarker of RNA oxidation, and its dependency on combustion sources. *Atmos. Environ.* **2019**, *213*, 444–455. [CrossRef]
61. Jiang, H.; Ahmed, C.M.; Canchola, A.; Chen, J.Y.; Lin, Y.H. Use of Dithiothreitol Assay to Evaluate the Oxidative Potential of Atmospheric Aerosols. *Atmosphere* **2019**, *10*, 571. [CrossRef]
62. Manigrasso, M.; Simonetti, G.; Astolfi, M.L.; Perrino, C.; Canepari, S.; Protano, C.; Antonucci, A.; Avino, P.; Vitali, M. Oxidative Potential Associated with Urban Aerosol Deposited into the Respiratory System and Relevant Elemental and Ionic Fraction Contributions. *Atmosphere* **2020**, *11*, 6. [CrossRef]
63. Borlaza, L.J.S.; Cosep, E.M.R.; Kim, S.; Lee, K.; Joo, H.; Park, M.; Bate, D.; Cayetano, M.G.; Park, K. Oxidative potential of fine ambient particles in various environments. *Environ. Pollut.* **2018**, *243*, 1679–1688. [CrossRef]
64. Adamson, I.Y.R.; Prieditis, H.; Vincent, R. Pulmonary Toxicity of an Atmospheric Particulate Sample Is Due to the Soluble Fraction. *Toxicol. Appl. Pharmacol.* **1999**, *157*, 43–50. [CrossRef]
65. Adamson, I.Y.R.; Prieditis, H.; Hedgecock, C.; Vincent, R. Zinc Is the Toxic Factor in the Lung Response to an Atmospheric Particulate Sample. *Toxicol. Appl. Pharmacol.* **2000**, *166*, 111–119. [CrossRef]
66. Voutsa, D.; Samara, C. Labile and bioaccessible fractions of heavy metals in the airborne particulate matter from urban and industrial areas. *Atmos. Environ.* **2002**, *36*, 3583–3590. [CrossRef]
67. Midander, K.; Pan, J.; Leygraf, C. Elaboration of a test method for the study of metal release from stainless steel particles in artificial biological media. *Corros. Sci.* **2006**, *48*, 2855–2866. [CrossRef]
68. Caboche, J.; Perdrix, E.; Malet, B.; Alleman, L.Y. Development of an in vitro method to estimate lung bioaccessibility of metals from atmospheric particles. *J. Environ. Monit.* **2011**, *13*, 621–630. [CrossRef]
69. McNeilly, J.D.; Heal, M.R.; Beverland, I.J.; Howe, A.; Gibson, M.D.; Hibbs, L.R.; MacNee, W.; Donaldson, K. Soluble transition metals cause the pro-inflammatory effects of welding fumes in vitro. *Toxicol. Appl. Pharmacol.* **2004**, *196*, 95–107. [CrossRef] [PubMed]
70. Donaldson, K.; Tran, L.; Jimenez, L.A.; Duffin, R.; Newby, D.E.; Mills, N.; MacNee, W.; Stone, V. Combustion-derived nanoparticles: A review of their toxicology following inhalation exposure. *Part. Fibre Toxicol.* **2005**, *2*, 10. [CrossRef] [PubMed]
71. Sauvain, J.-J.; Rossi, M.J. Quantitative Aspects of the Interfacial Catalytic Oxidation of Dithiothreitol by Dissolved Oxygen in the Presence of Carbon Nanoparticles. *Environ. Sci. Technol.* **2016**, *50*, 996–1004. [CrossRef]
72. Leclercq, B.; Alleman, L.Y.; Perdrix, E.; Riffault, V.; Happillon, M.; Strecker, A.; Lo-Guidice, J.-M.; Garçon, G.; Coddeville, P. Particulate metal bioaccessibility in physiological fluids and cell culture media: Toxicological perspectives. *Environ. Res.* **2017**, *156*, 148–157. [CrossRef]
73. Keane, M.; Stone, S.; Chen, B. Welding fumes from stainless steel gas metal arc processes contain multiple manganese chemical species. *J. Environ. Monit.* **2010**, *12*, 1133–1140. [CrossRef]
74. Hanley, K.W.; Andrews, R.; Bertke, S.; Ashley, K. Manganese Fractionation Using a Sequential Extraction Method to Evaluate Welders' Shielded Metal Arc Welding Exposures During Construction Projects in Oil Refineries. *J. Occup. Environ. Hyg.* **2015**, *12*, 774–784. [CrossRef]
75. Butler, O.; Musgrove, D.; Stacey, P. Preparation and Certification of Two New Bulk Welding Fume Reference Materials for Use in Laboratories Undertaking Analysis of Occupational Hygiene Samples. *J. Occup. Environ. Hyg.* **2014**, *11*, 604–612. [CrossRef]
76. Unceta, N.; Séby, F.; Malherbe, J.; Donard, O.F.X. Chromium speciation in solid matrices and regulation: A review. *Anal. Bioanal. Chem.* **2010**, *397*, 1097–1111. [CrossRef]
77. Pelfrêne, A.; Cave, M.R.; Wragg, J.; Douay, F. In Vitro Investigations of Human Bioaccessibility from Reference Materials Using Simulated Lung Fluids. *Int. J. Environ. Res. Public. Health* **2017**, *14*, 112. [CrossRef]
78. Hatch, G.E. *Comparative Biology of the Normal Lung*; Parent, R.A., Ed.; CRC Press: Boca Raton, FL, USA, 1992; pp. 617–632.
79. Lyu, Y.; Guo, H.; Cheng, T.; Li, X. Particle Size Distributions of Oxidative Potential of Lung-Deposited Particles: Assessing Contributions from Quinones and Water-Soluble Metals. *Environ. Sci. Technol.* **2018**, *52*, 6592–6600. [CrossRef] [PubMed]
80. Mbengue, S.; Alleman, L.; Flament, P. Size-distributed metallic elements in submicronic and ultrafine atmospheric particles from urban and industrial areas in northern France. *Atmos. Res.* **2014**, *135–136*, 35–47. [CrossRef]
81. Berlinger, B.; Weinbruch, S.; Ellingsen, D.G.; Zibarev, E.; Chashchin, V.; Chashchin, M.; Thomassen, Y. On the bio-accessibility of 14 elements in welding fumes. *Environ. Sci. Process. Impacts* **2019**, *21*, 497–505. [CrossRef] [PubMed]
82. Burgess, W. Potential exposures in the manufacturing industry—their recognition and control. In *Patty's Industrial*; Clayton, G.D., Clayton, F.E., Eds.; Wiley-Interscience: New York, NY, USA, 1991; pp. 595–674.
83. Keane, M.; Stone, S.; Chen, B.; Slaven, J.; Schwegler-Berry, D.; Antonini, J. Hexavalent chromium content in stainless steel welding fumes is dependent on the welding process and shield gas type. *J. Environ. Monit.* **2009**, *11*, 418–424. [CrossRef]
84. Berlinger, B.; Skogen, U.; Meijer, C.; Thomassen, Y. Workplace exposure to particulate matter, bio-accessible, and non-soluble metal compounds during hot work processes. *J. Occup. Environ. Hyg.* **2019**, *16*, 378–386. [CrossRef]
85. MétroPol. MétroPol M-43 (2016) Chrome VI. Available online: http://www.inrs.fr/publications/bdd/metropol/fiche.html?refINRS=METROPOL_43 (accessed on 19 October 2020).
86. Ruby, M.V.; Schoof, R.; Brattin, W.; Goldade, M.; Post, G.; Harnois, M.; Mosby, D.E.; Casteel, S.W.; Berti, W.; Carpenter, M.; et al. Advances in Evaluating the Oral Bioavailability of Inorganics in Soil for Use in Human Health Risk Assessment. *Environ. Sci. Technol.* **1999**, *33*, 3697–3705. [CrossRef]

87. Jenkins, N.T.; Pierce, W.M.-G.; Eagar, T. Particle size distribution of gas metal and flux cored arc welding fumes. *Weld. J.* **2005**, *84*, 156–163.
88. Jenkins, N.T. Chemistry of Airborne Particles from Metallurgical Processing. Ph.D. Thesis, Massachusetts Institute of Technology, Cambridge, MA, USA, September 2003.
89. Bau, S.; Rousset, D.; Payet, R.; Keller, F.-X. Characterizing particle emissions from a direct energy deposition additive manufacturing process and associated occupational exposure to airborne particles. *J. Occup. Environ. Hyg.* **2020**, *17*, 59–72. [CrossRef]
90. Mamede, A.-S.; Nuns, N.; Cristol, A.-L.; Cantrel, L.; Souvi, S.; Cristol, S.; Paul, J.-F. Multitechnique characterisation of 304 L surface states oxidised at high temperature in steam and air atmospheres. *Appl. Surf. Sci.* **2016**, *369*, 510–519. [CrossRef]
91. Feng, X.D.; Dang, Z.; Huang, W.L.; Yang, C. Chemical speciation of fine particle bound trace metals. *Int. J. Environ. Sci. Technol.* **2009**, *6*, 337–346. [CrossRef]
92. Daellenbach, K.R.; Uzu, G.; Jiang, J.; Cassagnes, L.-E.; Leni, Z.; Vlachou, A.; Stefenelli, G.; Canonaco, F.; Weber, S.; Segers, A.; et al. Sources of particulate-matter air pollution and its oxidative potential in Europe. *Nature* **2020**, *587*, 414–419. [CrossRef]
93. Park, M.; Joo, H.S.; Lee, K.; Jang, M.; Kim, S.D.; Kim, I.; Borlaza, L.J.S.; Lim, H.; Shin, H.; Chung, K.H.; et al. Differential toxicities of fine particulate matters from various sources. *Sci. Rep.* **2018**, *8*, 1–11. [CrossRef]
94. Rice, T.M.; Clarke, R.W.; Godleski, J.J.; Al-Mutairi, E.; Jiang, N.-F.; Hauser, R.; Paulauskis, J.D. Differential Ability of Transition Metals to Induce Pulmonary Inflammation. *Toxicol. Appl. Pharmacol.* **2001**, *177*, 46–53. [CrossRef] [PubMed]
95. Fujitani, Y.; Furuyama, A.; Tanabe, K.; Hirano, S. Comparison of Oxidative Abilities of PM2.5 Collected at Traffic and Residential Sites in Japan. Contribution of Transition Metals and Primary and Secondary Aerosols. *Aerosol Air Qual. Res.* **2017**, *17*, 574–587. [CrossRef]
96. Kachur, A.V.; Held, K.D.; Koch, C.J.; Biaglow, J.E. Mechanism of Production of Hydroxyl Radicals in the Copper-Catalyzed Oxidation of Dithiothreitol. *Radiat. Res.* **1997**, *147*, 409–415. [CrossRef] [PubMed]
97. Kumagai, Y.; Koide, S.; Taguchi, K.; Endo, A.; Nakai, Y.; Yoshikawa, T.; Shimojo, N. Oxidation of Proximal Protein Sulfhydryls by Phenanthraquinone, a Component of Diesel Exhaust Particles. *Chem. Res. Toxicol.* **2002**, *15*, 483–489. [CrossRef]
98. Krężel, A.; Leśniak, W.; Jeżowska-Bojczuk, M.; Młynarz, P.; Brasuñ, J.; Kozłowski, H.; Bal, W. Coordination of heavy metals by dithiothreitol, a commonly used thiol group protectant. *J. Inorg. Biochem.* **2001**, *84*, 77–88. [CrossRef]
99. Kaiwar, S.P.; Rao, C.P. In vitro reduction of Cr(VI) by low molecular weight biomimetic components: A comparative study using UV-Vis spectroscopy. *Chem. Biol. Interact.* **1995**, *95*, 89–96. [CrossRef]
100. Gustafsson, J.P. Visual MINTEQ 3.1. 2020. Available online: https://vminteq.lwr.kth.se/download/ (accessed on 4 May 2020).
101. Kohen, R.; Nyska, A. Oxidation of biological systems: Oxidative stress phenomena, antioxidants, redox reactions, and methods for their quantification. *Toxicol. Pathol.* **2002**, *30*, 620–650. [CrossRef]
102. Charrier, J.G.; Anastasio, C. Impacts of antioxidants on hydroxyl radical production from individual and mixed transition metals in a surrogate lung fluid. *Atmos. Environ.* **2011**, *45*, 7555–7562. [CrossRef] [PubMed]
103. Jin, K.; Park, J.; Lee, J.; Yang, K.D.; Pradhan, G.K.; Sim, U.; Jeong, D.; Jang, H.L.; Park, S.; Kim, D.; et al. Hydrated Manganese(II) Phosphate ($Mn_3(PO_4)_2.3H_2O$) as a Water Oxidation Catalyst. *J. Am. Chem. Soc.* **2014**, *136*, 7435–7443. [CrossRef] [PubMed]
104. Sigg, L.; Behra, P.; Stumm, W. *Chimie des Milieux Aquatiques—5e Edition: Cours et Exercices Corrigés*; Dunod: Malakoff, France, 1992; ISBN 978-2-10-059254-8.
105. Charrier, J.G.; McFall, A.S.; Vu, K.K.-T.; Baroi, J.; Olea, C.; Hasson, A.; Anastasio, C. A bias in the "mass-normalized" DTT response—An effect of non-linear concentration-response curves for copper and manganese. *Atmos. Environ.* **2016**, *144*, 325–334. [CrossRef] [PubMed]
106. Leonard, S.S.; Chen, B.T.; Stone, S.G.; Schwegler-Berry, D.; Kenyon, A.J.; Frazer, D.; Antonini, J.M. Comparison of stainless and mild steel welding fumes in generation of reactive oxygen species. *Part. Fibre Toxicol.* **2010**, *7*, 32. [CrossRef]
107. Verma, V.; Shafer, M.M.; Schauer, J.J.; Sioutas, C. Contribution of transition metals in the reactive oxygen species activity of PM emissions from retrofitted heavy-duty vehicles. *Atmos. Environ.* **2010**, *44*, 5165–5173. [CrossRef]
108. Lin, M.; Yu, J.Z. Effect of metal-organic interactions on the oxidative potential of mixtures of atmospheric humic-like substances and copper/manganese as investigated by the dithiothreitol assay. *Sci. Total Environ.* **2019**, *697*, 134012. [CrossRef]
109. Krawic, C.; Zhitkovich, A. Toxicological Antagonism among Welding Fume Metals: Inactivation of Soluble Cr(VI) by Iron. *Chem. Res. Toxicol.* **2018**, *31*, 1172–1184. [CrossRef]
110. Butler, O.; Musgrove, D. *Certification Report: Reference Material HSL SSWF-1, Elements in Stainless Steel Welding Fume, AS/2012/11*; Health and Safety Laboratory: Buxton, UK, 2012.
111. Butler, O.; Musgrove, D. *Certification Report: Reference Material HSL MSWF-1, Elements in Mild Steel Welding Fume, AS/2012/11*; Health and Safety Laboratory: Buxton, UK, 2012.
112. Rumble, J. *Archive Handbook of Chemistry and Physics 100st Edition*, 100th ed.; CRC Press: Boca Raton, FL, USA, 2019.